Mon. Not. R. astr. Soc. (1990) **242,** 318–337

The 60-μm and far-infrared luminosity functions of *IRAS* galaxies

W. Saunders,[1] M. Rowan-Robinson,[1] A. Lawrence,[1] G. Efstathiou,[2,4] N. Kaiser,[2,5] R. S. Ellis[3] and C. S. Frenk[3]

[1]*Astronomy Unit, Queen Mary College, Mile End Road, London E1 4NS*
[2]*Institute of Astronomy, Madingley Road, Cambridge CB3 0HA*
[3]*Department of Physics, South Road, Durham DH1 3LE*
[4]*Department of Astrophysics, Keble Road, Oxford OX1 3RH*
[5]*Canadian Institute for Theoretical Astrophysics, St George Street, Toronto, Ontario M5S 1A2, Canada*

Accepted 1989 June 30. Received 1989 June 27; in original form 1988 December 7

SUMMARY

The 60-μm luminosity function for galaxies detected by *IRAS* is determined from a compilation of samples with highly complete redshift information totalling 2818 galaxies, including the new QMC–Cambridge–Durham survey and samples including many nearby, low-luminosity galaxies. We use clustering-independent maximum likelihood methods throughout. A non-parametric estimator is used to determine the shape of the luminosity function, and the best parameter set found for a suitable analytic form. We find the luminosity function to be well described by a Gaussian dependence on log(luminosity), changing over to a very flat power law at low luminosities: this latter feature is in strong contrast to previous results. We find our results to be very insensitive to various models for deviations from the Hubble flow and to different values of the Hubble constant.

We present a generalization of the non-parametric estimator for determination of the bivariate luminosity function of samples defined by two flux limits. We apply this to two optically + 60-μm limited samples containing relatively large numbers of low-luminosity galaxies and confirm the flatness of the luminosity function at this end. The joint luminosity function suggests simple forms for the distribution of 60-μm luminosity versus blue luminosity and linear diameter, and we determine the maximum likelihood solutions for these forms. In addition, we determine the 40–120 μm far-infrared luminosity function, and derive separate 60-μm luminosity functions for the normal and starburst populations, as classified by far-infrared temperature.

We also present a new method for finding the run of density against distance for any flux and/or magnitude limited sample, independent of any assumptions on the shape of the luminosity function. Large local overdensities are found, confirming the existence of bias in previous work. This method forms an excellent indicator for evolution, and strong evolution [luminosity $\propto (1+z)^{3\pm1}$ or density $\propto (1+z)^{7\pm2}$] is seen in the QCD survey.

The combination of luminosity function and density estimator allows us to investigate the internal consistency of our results, and we find no evidence that systematic errors outweigh the statistical uncertainties.

1 INTRODUCTION

The *IRAS* survey has allowed the construction of the first homogeneously selected all-sky galaxy catalogues, with sufficient depth to look beyond known local superclustering. To make full use of the cosmological information in these samples, we require a reliable luminosity function over as large a range in luminosity as possible.

Redshifts, and hence luminosities, are known for about one third of the ~25 000 galaxies in the *Point Source Catalog*, mostly by identification with catalogued optical galaxies. However, determination of the luminosity function requires samples with well-defined selection criteria and highly complete redshift information, and hence we cannot hope to use more than a small fraction of the total data available.

Previous determinations of the luminosity function have been based on individual flux and area-limited surveys [Lawrence *et al.* 1986 (hereafter Paper II); Leech *et al.* 1988 (Paper IV); Soifer *et al.* 1986, 1987; Smith *et al.* 1987; Strauss & Huchra 1988; Vader & Simon 1987]. We have used all these surveys, together with the new QMC–Cambridge–Durham survey (Lawrence *et al.*, in preparation). We also use three other samples with well-defined joint infrared and optical or distance criteria; these are the diameter-limited *Large Galaxy Catalog* (Rice *et al.* 1988), the blue-magnitude-limited sample of Rowan-Robinson, Helou & Walker (1987, hereafter Paper III), and a new sample of nearby *IRAS* galaxies based on the KKT catalogue (Kraan-Kortweg & Tammann 1980). These latter samples are included in order to provide sufficient numbers of low-luminosity galaxies for determination of the faint end of the luminosity function. In total we have 2818 galaxies for this work. The luminosities cover seven decades, with reasonable statistics over five.

Published determinations of the luminosity function for galaxies detected by *IRAS* have used Schmidt's $\Sigma(1/V_{\max})$ estimator (Schmidt 1968) and least-χ^2 fitting of parametric forms, a method susceptible to two particular biases. First, methods involving fits to binned data will generally be biased if the data is not disturbed uniformly across the bins; this is the case for both the low and high ends of the luminosity function. Secondly, and more seriously, the method is biased by galaxy clustering. In particular, low-luminosity galaxies can only be seen out to modest distances; if our neighbourhood is overdense, the space density of such galaxies will be overestimated compared with more luminous and typically more distant ones. Most surveys to date look through the local supercluster, so this effect is particularly severe.

The STY parametric maximum-likelihood method (Sandage, Tammann & Yahil 1979) eliminates both the binning and clustering biases. A universal, parametrically defined shape for the luminosity function is assumed, with density variations only affecting the normalization. For a sample of galaxies with known distances, we can find, for any set of luminosity function parameters, the probability density function (or likelihood) for any given set of luminosities. The likelihood for the set of luminosities actually observed depends only on the parameters of the luminosity function, and the maximum likelihood solution is the set of parameters for which this is maximized. However, although for any given parametric form, the maximum likelihood parameter set can be found, there is no well-defined way of determining whether or not the form is really suitable, and different forms can only be compared by trial and error comparison of likelihoods.

This method has been applied to a large and highly complete sample of *IRAS* galaxies by Yahil (1987). Good evidence was found there in favour of the assumption of universality (which must in any case be implicitly assumed in any determination of the general luminosity function), and the luminosity function was satisfactorily described by a double power law over the range 10^8–10^{11} h^{-2} $L_\odot$. Nevertheless, we find that this form is not satisfactory over the much wider range of luminosities considered here.

The 'stepwise maximum likelihood' (SWML) method of Efstathiou, Ellis & Peterson (1988) (see also Nicoll & Segal 1983) is a generalization of the STY method whereby the luminosity function is taken to be an arbitrary step function; it is thus in effect non-parametric. While the resulting luminosity function is not physically plausible, it does allow absolute determination of the suitability of any parametric form chosen for application of the STY method, either by the likelihood ratio test of Efstathiou *et al.* (1988) or the χ^2 fits used here.

Throughout this paper, $\varphi(L)$ refers to the differential luminosity function per decade in luminosity, and $\Phi(L)$ to the number density of galaxies brighter than L, so $\varphi(L) = -d\Phi(L)/d\log L$.

In Section 2 we discuss the samples used, their completeness and flux accuracies. Section 3 explains our use of direct distances and bulk flow models to reduce the effects of deviations from uniform Hubble expansion. Section 4 describes the colour and K-corrections used in calculating the 60-μm and far-infrared luminosities. In Section 5 we describe the methods used for purely flux-limited samples. The results for these are presented in Section 6, together with a discussion on the possible systematic uncertainties associated with the flow models, Hubble constant and use of Local Group galaxies. In Section 7 we present general methods for dealing with jointly limited samples, and the resulting 60-μm and marginal luminosity functions for two optical and infrared limited samples containing relatively large numbers of low-luminosity galaxies.

In Section 8 we present a new method for finding the density against redshift distribution, not requiring prior knowledge of the selection function involved, and applicable to singly or jointly limited samples. In Section 9, we use this density estimator to investigate the internal consistency of our results. Finally, this density estimator forms an excellent indicator for evolution, and in Section 10 we fit simple evolutionary models and determine their effects on the parameters of the luminosity function.

2 THE DATA SET

Our basic data set is a new catalogue of *IRAS* galaxies containing 17 664 sources outside the Local Group and covering the 82 per cent of the sky outside the coverage gaps and regions with high source density. Sources are included on the basis of good or moderate quality fluxes in excess of 0.5 Jy at 60 μm, this being the wavelength where contamination from stars and cirrus is minimized (Rowan-Robinson *et al.* 1986, Paper I; Paper II). There are additional far-infrared colour and identification constraints to discriminate against cirrus, stars and planetary nebulae: these are listed in Appendix A. These constraints do not exclude any significant number of galaxies at $|b| > 20°$. Fluxes are taken in order of preference from the *Large Optical Galaxy Catalog* (Rice *et al.* 1988), the IRAS *Small Scale Structure Catalog* (SSSC, 1988), and the IRAS *Point Source Catalog,* Version 2 (PSC2, 1988).

We have used this catalogue to re-select all samples (except S8 below) from areas and flux-ranges where extensive redshift data exist. The survey on which each sample is based and the selection criteria used are as follows:

S1. The survey of bright *IRAS* galaxies by Soifer *et al.* (1987). 328 sources with $S_{60} \geqslant 5.0$ Jy over 14 500 deg^2.
S2. The study of a flux-limited sample of *IRAS* galaxies by

Smith *et al.* (1987). 70 galaxies with $S_{60} \geqslant 2.0$ Jy over 1072 deg^2.

S3. The North Galactic Wedge survey (NGW); that is the study of *IRAS* sources at high galactic latitude by Lawrence *et al.* (Paper II), and its extension as part of the QCD survey. 389 sources with $S_{60} \geqslant 0.60$ Jy over 844 deg^2.

S4. The Bootes void survey (Strauss & Huchra 1988). 379 galaxies with $S_{60} \geqslant 0.75$ Jy over 1423 deg^2.

S5. The new QMC–Cambridge–Durham (QCD) survey (Lawrence *et al.* 1989); a 1 in 6 random selection consisting of 2387 galaxies with $S_{60} \geqslant 0.6$ Jy, covering 30 500 deg^2. For maximal completeness, we have used only the 1787 galaxies with $|b| > 20°$.

S6. The Vader & Simon/KOSS redshift sample (Vader & Simon 1987). 63 galaxies with $S_{60} \geqslant 0.6$ Jy in 7 scattered fields covering 142 deg^2.

S7. *IRAS* galaxies in the KKT catalogue (Kraan–Kortweg & Tammann 1980, as revised by Huchtmeier & Richter (1986). 55 galaxies with $V \leqslant 500$ km s^{-1}, $S_{60} \geqslant 0.6$ Jy and $|b| > 20°$. Included in this sample are the Local Group galaxies listed in the *IRAS* Explanatory Supplement (Beichman *et al.* 1984); these are listed in Table 1.

Table 1(a). Local Group members used.

Name	Distance (Mpc)	S_{60}(Jy)	Flux Source	log ($L_{60}/L_\odot$)
I10	1.30	70.47	SSSC	8.56
N185	0.68	0.31	LGC	5.56
N205	0.68	0.60	LGC	5.84
M31	0.68	536.18	LGC	8.81
SMC	0.06	6688.91	LGC	7.88
I1613	0.69	1.42	LGC	6.30
M33	0.66	419.65	LGC	8.73
LMC	0.05	82917.00	LGC	8.72
N6822	0.55	47.63	LGC	7.65
I5152	1.50	4.30	SSSC	7.48
A2359	0.95	0.32	LGC	5.93

Distances are from Richter *et al.* (1987). SSSC = IRAS *Small Scale Structure Catalog* (1988), LGC = *Large Optical Galaxy Catalog* (Rice *et al.* 1988).

Table 1(b). Direct distances used for nearby groups of galaxies.

Name	Assumed Distance (Mpc)	No. of members used
Sculptor	2.2	6
M81 group	3.1	11
Virgo	19.0	115
M101 group	6.7	4
N5128 group	4.1	6

Distances are from Rowan-Robinson (1989).

S8. The catalogue by Rice *et al.* (LGC, 1988), contains 67 galaxies with $S_{60} \geqslant 0.25$ Jy, blue major diameters D_{25} greater than 8 arcmin (in the system of the *Revised Catalogue of Bright Galaxies*, de Vaucouleurs, de Vaucouleurs & Corwin 1976 (RC2)) and $|b| > 20°$.

S9. The study of IRAS *Galaxies at High Galactic Latitudes* (Paper III). 416 galaxies with $S_{60} \geqslant 0.6$ Jy and $m_B \leqslant 14.1$ over 2763 deg^2, where m_B is the corrected Zwicky magnitude.

Fig. 1 shows the distribution of these surveys on the sky, and it can be seen that the surveys are heavily biased towards the northern galactic hemisphere. The methods we use for determination of the luminosity function, however, are unaffected by clustering or local overdensity, and normalization is from the entire *IRAS* catalogue. All that follows rests, in any case, on the existence of a universal luminosity function; as long as this holds, no bias is introduced by this weighting towards the north.

We also have a great deal of overlap: our 3554 'sources' represent only 2818 distinct galaxies (we will keep to this nomenclature throughout). Counting a galaxy as two or more sources in different samples does not lead to any bias in the determination of the luminosity function, but will cause the 1σ errors to be slightly underestimated. We therefore recalculate the error taking this multiplicity into account.

The uncertainty in the fluxes is of the order of 10 per cent (Beichman *et al.* 1984; Rice *et al.* 1988) except for the 141 galaxies with fluxes taken from the SSC catalogue, where the uncertainty is of order 30 per cent (Rowan-Robinson 1988). There are also 114 galaxies flagged as extended at 60 μm but with fluxes taken from the PSC2; some at least of these will have had their fluxes underestimated. This underestimation is typically 20 per cent and occasionally as much as 50 per cent of the flux obtained by add-scanning over the source, but these sources represent only a small fraction ($\leqslant 20$ per cent) of the galaxies in any luminosity bin in our final non-parametric solution.

PSC2 detections are by definition unresolved by the *IRAS* beam; pairs or groups of galaxies closer together than ~ 2 arcmin will be seen as one object, and assigned a single flux and luminosity. This effect becomes significant at high luminosities, due to the large redshifts (and hence large unresolved projected separations) and the intrinsically interactive nature of many of these sources (Lawrence *et al.* 1989; Sanders *et al.* 1988). Our results strictly apply only to objects as seen by *IRAS*, rather than to galaxies as they would be defined optically. The luminosity function for the latter would be slightly steeper at the high-luminosity end.

Each sample is more than 95 per cent complete, and our overall completeness for the combined sample is better than 98 per cent. Further , many of the galaxies without redshifts are simply unobserved, rather than optically faint, empty fields or galaxies with featureless spectra (so no strong bias against unusual sources is introduced). Apart from sample S8, where each source has been add-scanned, none of our lower flux limits is below 0.6 Jy, so the degree of incompleteness carried over from the PSC2 should be very small (Beichman *et al.* 1984).

3 DISTANCES

Given the accuracy of the *IRAS* fluxes, the major uncertainty in our calculated luminosities comes from the distance

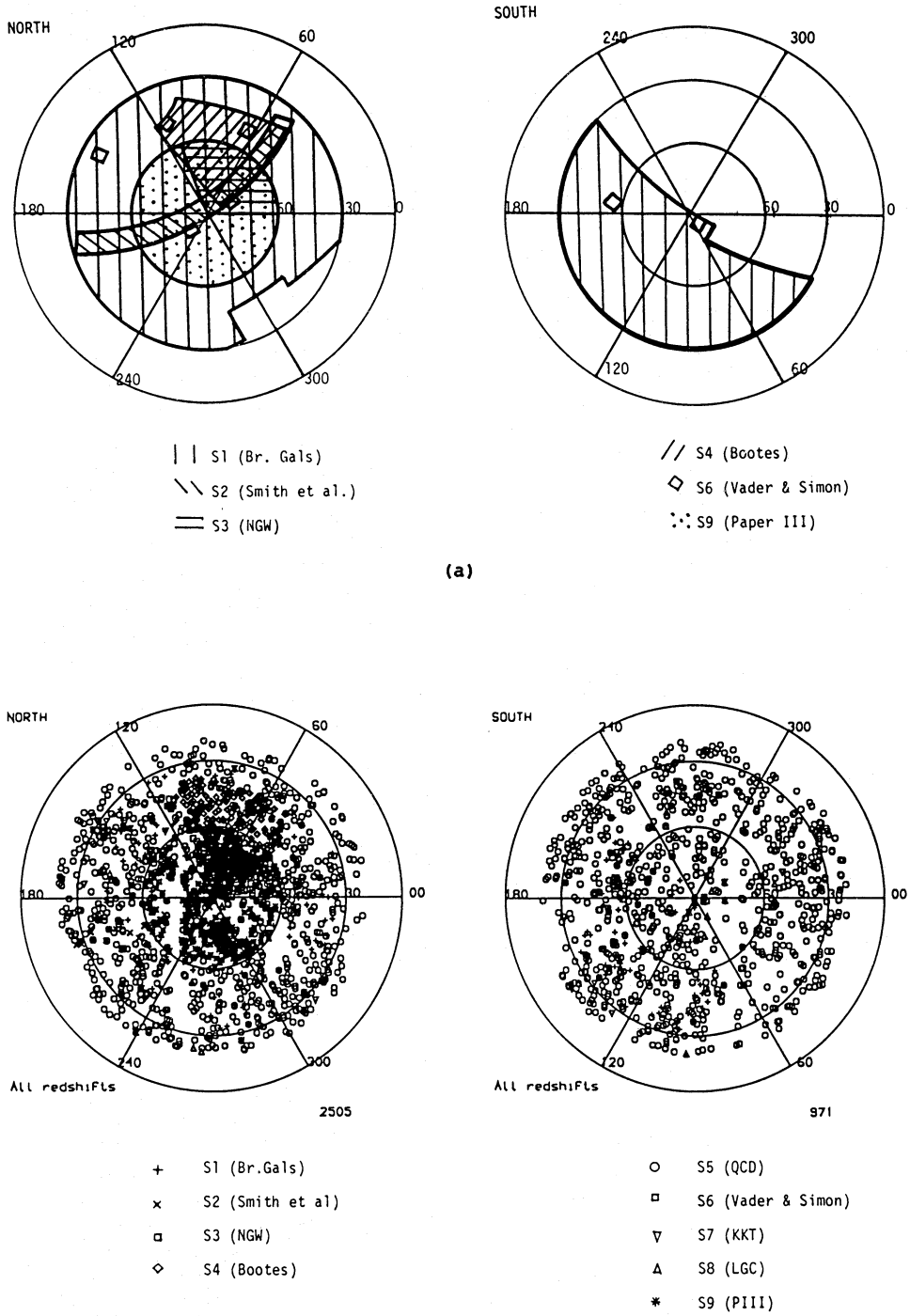

Figure 1. (a) Area of each survey plotted in equal-area galactic coordinates. Samples S5 (QCD), S7 (KKT) and S8 (LGC) are all-sky at $|b| > 20°$.

assigned to each galaxy. The relationship between redshift and distance is affected by the value of the Hubble constant, by peculiar 'thermal' velocities, and by large-scale bulk flows. We have used directly measured distances rather conservatively, that is only for galaxies where the peculiar velocity is evidently of the same order as or larger than the Hubble velocity. In addition, we have used direct distances for nearby groups only where this distance is reasonably secure, that is with 1σ uncertainty in the distance modulus less than 0.5 mag (Rowan-Robinson 1989). There are other galaxies for which the velocity is probably a poor measure of distance, but this seems less serious than the possibility of introducing systematic biases through uncertain group distances or membership, or using a distance indicator such

as the Tully–Fisher relation whose dispersion and zero-point are controversial. The galaxies and groups for which we have used direct distances are listed in Table 1. For the rest of the data set we use the most accurate redshift available, together with a correction for the motion of the Sun with respect to the centroid of the Local Group of 300 $\sin(l)\mathrm{b}\cos(b)$ km s^{-1} (de Vaucouleurs *et al.* 1979). This is converted to a luminosity distance using $H_0 = 66$ km s^{-1} Mpc^{-1} (Rowan-Robinson 1989) unless otherwise specified; this value is used to ensure consistency with the direct distances above.

Finally, there is considerable uncertainty in the distances of the galaxies due to bulk deviations from the Hubble flow. We have used a variety of simple flow models to try to correct for the largest systematic effects; these models are listed in Appendix B. Our default flow model (V3) has infall towards Virgo inversely proportional to distance; Virgo is assumed to be at distance $D_{\mathrm{Vir}} = 19.0$ Mpc (Rowan-Robinson 1989) and the infall at the Local Group is taken to be 220 km s^{-1} (Tammann & Sandage 1985). All galaxies in the triple-valued zone defined by this model are assigned distance D_{Vir}. In addition, we have included a Microwave Background contribution of 600 km s^{-1} towards $(l, b) = (268,27)$ (Lubin & Villela 1986); this is blended in between D_{Vir} and $3 \times D_{\mathrm{Vir}}$ from the Local Group, such that nearby galaxies share our MWB velocity, while distant galaxies are at rest with respect to the MWB. The variation in our final determined parameters due to different flow models is very small (much less than the formal errors), so we believe these models are adequate for the present purposes.

All our results are quoted in terms of $h = H_0/100$ km s^{-1} Mpc^{-1}. Our use of both direct distances for nearby galaxies, and redshift-derived distances otherwise, means that the shape of our resulting luminosity function is slightly dependent on the value of H_0 used in the calculations, even after this renormalization is performed. A cosmological model with $\Omega = 1$ and $\Lambda = 0$ has been used throughout this paper.

4 COLOUR AND K-CORRECTIONS

All but 290 of our sources have good- or moderate-quality fluxes at 100 μm in addition to those at 60 μm; we assign 100-μm fluxes to the remainder by fitting the S_{100}/S_{60} ratio as a function of 60-μm luminosity, as explained in Appendix C.

We assume that the spectrum of each source is given by a single-temperature Planck function multiplied by an emissivity proportional to wavelength; the investigation by Rowan-Robinson & Crawford (1989) suggests this to be a satisfactory description of the spectrum in the range 60–100 μm for disc-dominated emission, and a reasonable approximation for starburst-dominated emission.

For each source, then, we fit a single-temperature, $S_\nu \propto \nu B_\nu(T_{\mathrm{obs}})$ curve such that the spectrum convolved with the detector responses (as listed by Beichman *et al.* 1984) gives the observed broadband fluxes. From T_{obs} we find an emission temperature $T_{\mathrm{em}} = T_{\mathrm{obs}}(1+z)$, and also $S_{60\mathrm{em}}$, the monochromatic flux per hertz received at $60(1+z)$ μm. L_{60} is then defined as νP_ν at 60 μm in the galaxy rest frame, where

$$P_\nu = \frac{S_{60\mathrm{em}}}{(1+z)} 4\pi d_{\mathrm{l}}^2 \tag{4.1}$$

and, for $\Omega = 1$ and $\Lambda = 0$,

$$d_{\mathrm{l}} = \frac{2c}{H_0}\left(-\frac{1}{\sqrt{(1+z)}}\right)(1+z). \tag{4.2}$$

From T_{obs} and $S_{60\mathrm{em}}$ we calculate F_{fir}, the total flux received between $42.5(1+z)$ and $122.5(1+z)$ μm, and hence L_{fir}, the luminosity emitted between 42.5 and 122.5 μm, i.e.

$$L_{\mathrm{fir}} = 4\pi d_{\mathrm{l}}^2 F_{\mathrm{fir}}. \tag{4.3}$$

All luminosities are calculated in terms of $L_\odot = 3.826 \times 10^{33}$ erg s^{-1}.

Previous work has mostly used a K-correction assuming $S_\nu \propto \nu^\alpha$, $\alpha = -2$, based on average values of S_{25}/S_{60} and S_{60}/S_{100}. Because we fit a convex curve to S_{60} and S_{100}, we find that the slope of the spectrum at 60 μm tends to be steeper than this. In addition, the colour corrections generally increase the quoted fluxes: our derived luminosities are then slightly higher than those used in, for example, Paper II. For straightforward calculation of the selection function applicable to the *IRAS* catalog we have also derived the luminosity function based on a straight K-correction with $\alpha = -2$ and no colour correction (solution 19 of Table 3).

5 METHODS FOR PURELY FLUX-LIMITED SAMPLES

5.1 Maximum-likelihood parameter estimation

Suppose we have a data set $X_1, \ldots, X_n$ drawn from unknown parent distributions $f_1(x_1), \ldots, f_n(x_n)$. Then, if each f_i depends only on parameters $\theta_1, \ldots, \theta_m$, we can assign a likelihood l_i to each X_i: $l_i(\theta_1, \ldots, \theta_m) = f_i(X_i)$; the likelihood for the entire data set is $\mathscr{L}(\theta_1, \ldots, \theta_m) = \Pi\, l_i$. The maximum-likelihood solution for $\{\theta_1, \ldots, \theta_m\}$ is simply the set giving the maximum value for $\mathscr{L}$; that is the parameter set making the observed data set 'most probable'.

5.2 The Sandage, Tammann & Yahil method

The STY method (Sandage *et al.* 1979) starts from the assumption that the distribution of galaxies in space and luminosity is separable into a universal luminosity function $\varphi(L)$ and a normalization $\rho(\boldsymbol{r})$ reflecting density variations (including density evolution). The number density of galaxies at $\boldsymbol{r}$, per decade in luminosity, at luminosity L is then

$$n(L, \boldsymbol{r}) = \rho(\boldsymbol{r})\,\varphi(L). \tag{5.1}$$

At distance $\boldsymbol{r}$ there is a minimum luminosity L_{min} for a source to be included in a flux-limited catalogue. The number density of sources with $L > L_{\mathrm{min}}$ is

$$N(L_{\mathrm{min}}, \boldsymbol{r}) = \int_{L_{\mathrm{min}}}^{\infty} n(L, \boldsymbol{r})\, d\log L = \rho(\boldsymbol{r})\,\Phi(L_{\mathrm{min}}), \tag{5.2}$$

where

$$\Phi(L) = \int_{L}^{\infty} \varphi(L')\, d\log L'. \tag{5.3}$$

Suppose a source is in a sample at position $\boldsymbol{r}_i$, and that $L_{\mathrm{min},i}$ is the corresponding minimum luminosity. The parent

distribution of possible luminosities is then independent of the density at $\boldsymbol{r}$,

$$f_i(L) = \frac{n(L,\boldsymbol{r}_i)}{N(L_{\min,i},\boldsymbol{r}_i)} = \frac{\varphi(L)}{\Phi(L_{\min,i})} \quad \text{for } L > L_{\min,i},$$

$$= 0 \text{ otherwise.} \tag{5.4}$$

For any given functional form for φ depending on a set of parameters $\{\theta_1, \theta_2, \ldots, \theta_m\}$, $l_i = f(L_i)$, and hence $\mathscr{L} = \Pi\, l_i$, is a function only of the m variables in this parameter set. The set $\{\theta_1, \theta_2, \ldots, \theta_m\}$ giving a maximum for $\mathscr{L}$ forms the maximum-likelihood solution for the particular parametrized form chosen.

For a maximum-likelihood estimate $\{\theta_j\}$ of the true parameter set $\{\theta_j'\}$, the distribution of $\{\theta_j - \theta_j'\}$ is asymptotically multivariate Gaussian with zero mean and covariance matrix given by inversion of the matrix of second derivatives $\{-\partial^2 \ln \mathscr{L}/\partial\theta_j \partial\theta_k\}$ (Kendall & Stuart 1979). Hence the statistical errors are approximately Gaussian, and a 1σ uncertainty corresponds to $\Delta \ln \mathscr{L} = -\frac{1}{2}$. Because there is multiplicity in our combined data set, this procedure slightly underestimates the true statistical errors. We therefore assign each source a weight w_i in accordance with its multiplicity (e.g. a source appearing in three samples is given a weight $\frac{1}{3}$ in each), and recalculate the second derivatives using $\ln \mathscr{L}' = \Sigma\, w_i \ln l_i$.

5.3 Non-parametric maximum likelihood estimator

The 'Stepwise Maximum Likelihood Method' (Efstathiou *et al.* 1988) is similar in principle, with φ now an arbitrary non-negative step function in bins of log L. Then we have

$$\frac{\partial \ln \mathscr{L}}{\partial \varphi_j} = \frac{n_j}{\varphi_j} - \Sigma \frac{f_{ij}}{\Phi(L_{\min,i})}, \tag{5.5}$$

where φ_j is the value of φ in the jth luminosity bin, n_j is the number of sources in the bin, f_{ij} is the fraction of the bin contained in $[\log(L_{\min,i}), \infty]$, and the sum is over all sources in the sample. The maximum-likelihood solution $\{\varphi_j\}$ then has, for each j,

$$\varphi_j = n_j \left[\Sigma \frac{f_{ij}}{\Phi(L_{\min,i})} \right]^{-1}. \tag{5.6}$$

We use this to find an iterative solution for $\{\varphi_j\}$; typically this takes 20–30 iterations to achieve three significant figures for all bins.

Our quoted results use bin widths of 0.2 in log L_{60}. The results are insensitive to this, except for samples with an upper as well as a lower flux limit and a range in possible fluxes comparable to the bin size. Also, for all maximum-likelihood methods, an upper flux limit drastically reduces the available range in luminosity for each source; consequently the likelihood is rather insensitive to the parameter values. This is why we have not tried to cut our samples into non-overlapping flux and area ranges; to do so would throw information away, and in the limiting case of vanishingly small flux intervals we are left with no usable information.

Either end of the luminosity function may become 'decoupled' from the rest. This will happen if for any bin, b_j, there are no sources with $b_{\min,i} \leqslant b_j < b_i$ (b_i is the luminosity bin for the ith source etc). It is not necessary to have sources in every bin, and equation (5.6) gives $\varphi_j = 0$ for empty bins.

Variances and covariances between bins are found by inverting the matrix of second derivatives subject to some constraint on φ_j, e.g. $\Sigma\, \varphi_j L_j^{\beta} = \text{constant}$ (Efstathiou *et al.* 1988); in practice the cross-derivatives are small and we set them equal to zero. We recalculate the second derivatives at the solution, weighting the sources as above.

The errors for each φ_j are strongly asymmetric when n_j is small. If we vary φ_j from its maximum-likelihood value φ_j', keeping all other φ_k fixed, we have

$$\Delta \ln \mathscr{L}(\varphi_j) = \ln \mathscr{L}(\varphi_j) - \ln \mathscr{L}(\varphi_j')$$

$$\approx n_j \left(\ln \frac{\varphi_j}{\varphi_j'} - \frac{\varphi_j}{\varphi_j'} + 1 \right). \tag{5.7}$$

However, for φ_j in the range of interest, say $\ln \mathscr{L}(\varphi_j) \geqslant \ln(\varphi_j') - 1$, $\ln \mathscr{L}(\varphi_j)$ is nearly symmetric in $\ln(\varphi_j/\varphi_j')$ and close to the form expected if the error in this is Gaussian even for $n_j = 1$; hence we take our errors to be in $\ln \varphi_j$. Our statistical errors are then

$$\sigma(\ln \varphi_j) = \left(\frac{-\partial^2 \ln \mathscr{L}'}{\partial \ln \varphi_j^2} \right)^{-1/2}$$

$$= \frac{1}{\varphi_j} \left\{ \frac{\Sigma\, w_i}{\varphi_j^2} - \sum_i w_i \left(\frac{f_{ij}}{\Phi(L_{\min,i})} \right)^2 \right\}^{-1/2}, \tag{5.8}$$

where the first summation is over sources in bin j, and the second is over all sources.

If $n_j = 0$, $\partial \ln \mathscr{L}/\partial \varphi_j \neq 0$ at $\varphi_j = 0$, and so equation (5.8) does not apply. However, we can find a crude upper limit to φ_j by again demanding that $\ln \mathscr{L}(\varphi_j) = \ln \mathscr{L}(0) - \frac{1}{2}$. We use the first and second derivatives of $\mathscr{L}$ with respect to φ_j at $\varphi_j = 0$ to find this; the second derivatives are small, and hence

$$\varphi_{j,\max} \simeq \tfrac{1}{2} / \Sigma [f_{ij}/\Phi(L_{\min,i})], \tag{5.9}$$

and our upper limit broadly corresponds to $n_j = \frac{1}{2}$. The errors are hopelessly non-Gaussian and we use this limit for graphical purposes only.

5.4 Reliability of maximum-likelihood methods

Maximum-likelihood methods are in general only asymptotically unbiased (see the discussion by Efstathiou *et al.* 1988 for full details). We have run our luminosity function programs on random data sets, both with and without density dependence on z; the derived luminosity functions and errors are in good agreement with those from which the random data sets were derived.

Because maximum-likelihood methods work in effect by finding the slope of the luminosity function at any point, there is a rather high sensitivity to some forms of systematic errors. In particular, suppose a sample is incomplete near its lower flux limit. Then, at any luminosity, the number of sources close to that luminosity will be underestimated, and hence the slope of the luminosity function will also be underestimated. It is because of this effect that we have not used any data below 0.6 Jy. It is possible that some nearby,

optically faint *IRAS* sources are not included in the KKT catalogue and, if so, sample S7 will suffer from this effect, although we will see in Section 7 that this is not expected to be significant.

5.5 Adequacy of maximum-likelihood solutions

It should be noted that the errors derived above for the STY method are *relative* only; for a given parameter set we can exclude all sets of parameters outside some region of parameter space because their likelihoods are sufficiently worse than that of a known solution. However, we can never be sure that there are not other forms giving better likelihoods, and hence possibly excluding the entire parametric representation.

For the SWML solution, the same is in principle true, but now our parameter space includes all possible step functions (for a given binning scheme). Because the error in each $\ln \varphi_j$ is approximately Gaussian with known variance, even for small n_j, we can perform a χ^2 test on any given parametric expression for $\varphi(L)$. The expected value of φ_j is

$$E(\varphi_j)=\frac{\int V_{\max}(L)\varphi(L)}{\int V_{\max}(L)} \approx \frac{\int L^{3/2}\varphi(L)}{\int L^{3/2}},$$

where the integrals are over the bin. If $\varphi(L)$ is the true luminosity function, the distribution of $\Sigma \ln^2[\varphi_j/E(\varphi_j)]/\sigma_j(\ln \varphi_j)^2$ (over all bins) will then follow a standard χ^2 distribution with one less degree of freedom than the number of bins (because the relative normalization is arbitrary), and we can use this as an *absolute* test of the suitability of a given parametric solution.

5.6 Normalization

Both the STY and SWML methods lose the overall normalization for φ; for *IRAS* galaxies this is not really a problem as there are well-determined source-counts. We normalize the luminosity function by demanding that the total number of sources with $S_{60} \geqslant 0.60$ Jy be 1397 sr^{-1} (Rowan-Robinson & Saunders, in preparation), but there is no rigorous way of determining the uncertainty in this number without a detailed investigation of the clustering of *IRAS* galaxies on very large scales. However, it is reasonable to assume that it is of the same order as the number dipole, that is about 5 per cent.

The source counts have to be corrected for evolution: we want the normalization for the local luminosity function at the present epoch, while the source counts come from all redshifts. For the evolutionary models investigated in Section 10, this correction amounts to 25 per cent with uncertainty of 9 per cent. We have then taken the uncertainty in the overall normalization to be ±10 per cent.

6 RESULTS AND DISCUSSION FOR PURELY FLUX-LIMITED SAMPLES

6.1 60-μm luminosity function

The resulting SWML luminosity function for each of samples S1–S7 is shown in Fig. 2, as is the solution when they are treated as a single combined sample, and the values for this are given in Table 2.

Table 2. Combined non-parametric 60 μm luminosity functions.

	Combined Total, S1-S7			Combined Total, S1-S9		
logL	n_{tot}	n_{gal}	φ(L)	n_{tot}	n_{gal}	φ(L)
5.1	0	0	0.00(0.92)E-1	0	0	0.00(0.91)E-1
5.3	0	0	0.00(0.92)E-1	1	1	0.40(0.42)E-1
5.5	1	1	0.14(0.18)E-0	2	1	0.60(0.70)E-1
5.7	0	0	0.00(0.21)E-1	1	1	0.33(0.36)E-1
5.9	0	0	0.00(0.18)E-1	0	0	0.00(0.18)E-1
6.1	1	1	0.34(0.38)E-1	2	1	0.34(0.37)E-1
6.3	0	0	0.00(0.17)E-1	0	0	0.00(0.17)E-1
6.5	0	0	0.00(0.14)E-1	0	0	0.00(0.14)E-1
6.7	0	0	0.00(0.88)E-2	0	0	0.00(0.88)E-2
6.9	1	1	0.10(0.11)E-1	1	1	0.10(0.11)E-1
7.1	0	0	0.00(0.30)E-2	1	1	0.11(0.12)E-1
7.3	5	5	0.20(0.09)E-2	7	5	0.24(0.12)E-1
7.5	2	2	0.57(0.41)E-2	3	3	0.76(0.46)E-2
7.7	10	7	0.19(0.08)E-1	14	7	0.19(0.08)E-1
7.9	9	6	0.12(0.05)E-1	12	7	0.11(0.05)E-1
8.1	8	6	0.92(0.40)E-2	14	9	0.90(0.33)E-2
8.3	16	10	0.14(0.05)E-1	20	12	0.11(0.35)E-1
8.5	12	12	0.71(0.21)E-2	27	21	0.72(0.17)E-2
8.7	23	18	0.75(0.19)E-2	59	45	0.87(0.14)E-2
8.9	43	35	0.88(0.17)E-2	71	49	0.72(0.11)E-2
9.1	41	36	0.55(0.10)E-2	75	55	0.55(0.08)E-2
9.3	78	68	0.57(0.07)E-2	130	103	0.59(0.06)E-2
9.5	123	99	0.46(0.05)E-2	170	114	0.45(0.05)E-2
9.7	165	138	0.32(0.03)E-2	226	152	0.35(0.03)E-2
9.9	207	172	0.22(0.02)E-2	248	180	0.22(0.02)E-2
10.1	250	209	0.14(0.01)E-2	297	225	0.15(0.01)E-2
10.3	304	270	0.82(0.06)E-3	334	284	0.82(0.06)E-3
10.5	348	291	0.44(0.03)E-3	373	299	0.45(0.03)E-3
10.7	344	291	0.23(0.02)E-3	362	294	0.23(0.02)E-3
10.9	270	229	0.10(0.08)E-3	280	232	0.11(0.08)E-3
11.1	231	199	0.46(0.04)E-4	233	198	0.45(0.04)E-4
11.3	174	155	0.19(0.02)E-4	175	155	0.19(0.02)E-4
11.5	119	104	0.67(0.08)E-5	120	104	0.66(0.08)E-5
11.7	85	68	0.25(0.04)E-5	85	68	0.25(0.04)E-5
11.9	57	52	0.83(0.14)E-6	57	52	0.83(0.14)E-6
12.1	38	32	0.30(0.06)E-6	38	32	0.29(0.06)E-6
12.3	29	22	0.11(0.03)E-6	29	22	0.11(0.03)E-6
12.5	5	5	0.44(0.26)E-8	5	5	0.44(0.29)E-8
12.7	3	2	0.15(0.13)E-8	3	2	0.14(0.13)E-8
12.9	0	0	0.00(0.25)E-9	0	0	0.00(0.25)E-9

Combined non-parametric solutions for all flux-limited samples (S1–S7), and including the two jointly limited samples (S1–S9). L is in units of $L_\odot$ for $H_0=66$ km s^{-1} Mpc^{-1}, and $\varphi(L)$ is in units of Mpc^{-3} dex^{-1}. n_{tot} is the number of sources used in the calculation, n_{gal} is the actual number of galaxies. The 1σ error is in brackets; this should strictly be considered as referring to the error in $\ln \varphi$, i.e. $\sigma(\ln \varphi)=\sigma_{quoted}/\varphi$. Where $\varphi=0$, the quoted error is an upper limit to φ as explained in the text. Calculated with flow model V3 and no evolutionary correction.

None of the traditional parametric forms for luminosity functions are a suitable description. A Schechter function is too narrow, while the Gaussian form proposed by Sandage, Binggeli & Tammann (1985) for spirals does not match the faint end satisfactorily. The two power-law forms of Paper II and Yahil (1987) fail to describe the continued curvature over several decades in L_{60}.

We have, then, found STY solutions with φ represented by the function

$$\varphi(L)=C\left(\frac{L}{L_*}\right)^{1-\alpha}\exp\left[-\frac{1}{2\sigma^2}\log_{10}^2\left(1+\frac{L}{L_*}\right)\right], \quad (6.1)$$

which behaves as a power law for $L \ll L_*$ and as a Gaussian in $\log L$ for $L \gg L_*$. This form appears to match the data adequately, and has the same number of parameters (four) as

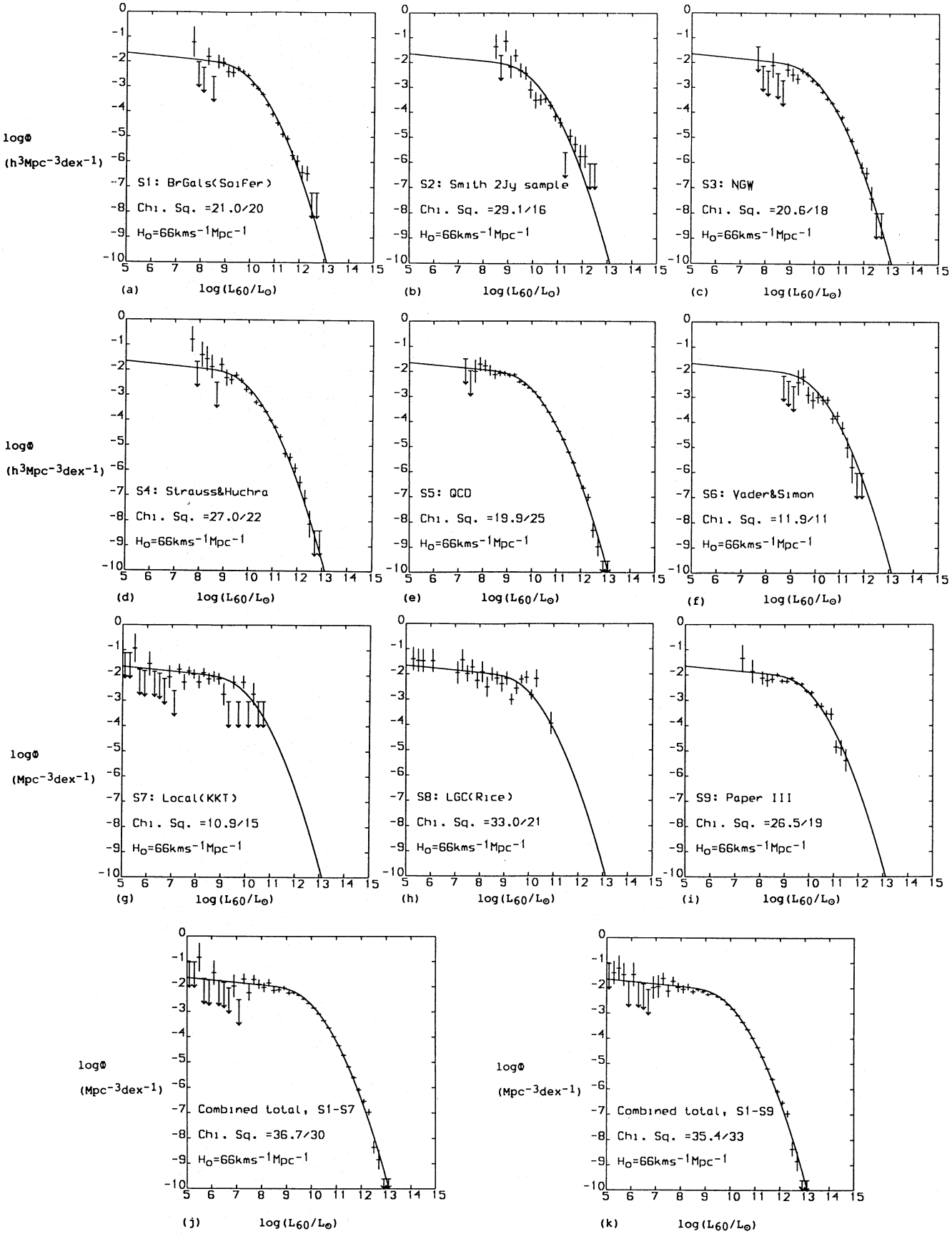

Figure 2. Non-parametric luminosity functions for each sample (a–i), and for combined samples (j), (k). The χ^2 is between this non-parametric solution and the final parametric solution as described in the text; this is the curve on each plot. All points and lines calculated with far-infrared temperature-based K-corrections, flow model V3, $H_0 = 66$ km s^{-1} Mpc^{-1}, $\Omega = 1$, $\Lambda = 0$.

Table 3(a). Parametric solutions.

Soln. no.	Sample	α	σ	log $(L_*/h^{-2}L_\odot)$	C $(h^3\mathrm{Mpc}^{-3})$
1	S1 (Br. Gal. Cat.)	1.01	0.750	8.22	3.4E-2
2	S2 (Smith et al.)	(1.10)	0.768	(8.47)	1.9E-2
3	S3 (North Gal. Wedge)	(1.10)	0.753	(8.47)	2.1E-2
4	S4 (Strauss and Huchra)	(1.10)	0.744	(8.47)	2.3E-2
5	S5 (QCD Survey)	1.15	0.699	8.60	2.6E-2
6	S6 (Vader & Simon)	(1.10)	0.718	(8.47)	2.9E-2
7	S7 (KKT)	1.10	(0.724)	(8.47)	2.7E-2
8	S8 (Large. Gal. Cat)	1.10	(0.724)	(8.47)	2.7E-2
9	S9 (Paper III)	1.05	(0.724)	8.47	2.2E-2
10	S1-S7, Flow model V1	1.06	0.738	8.34	3.2E-2
11	S1-S7, Flow model V2	1.08	0.721	8.48	2.6E-2
12	**S1-S7, Flow model V3**	**1.09**	**0.724**	**8.47**	**2.6E-2**
13	S1-S7, Flow model V4	1.09	0.716	8.52	2.3E-2
14	S1-S7, Flow Model V5	1.09	0.718	8.50	2.5E-2
15	S1-S7, Flow Model V6	1.08	0.724	8.45	2.6E-2
16	S1-S7, Flow Model V7	1.08	0.723	8.47	2.6E-2
17	S1-S7, H_0 = 50	1.13	0.723	8.51	2.6E-2
18	S1-S7, H_0 = 100	1.05	0.720	8.44	2.5E-2
19	S1-S7, α = -2	1.08	0.726	8.41	3.0E-2
20	S1-S7, extended ×2	1.08	0.724	8.47	2.5E-2
21	S1-S7, No Local Group	1.12	0.721	8.52	2.6E-2
22	S1-S7, Vel > 500kms^{-1}	0.92	0.727	8.23	2.6E-2
23	S1-S7, Q = 3.1, P = 0	1.09	0.711	8.45	2.8E-2
24	Cool (<36K),S1-S7	1.15	0.463	9.02	1.6E-2
25	Warm (>36K),S1-S7	1.27	0.626	9.39	2.6E-3
26	L_{fir}, S1-S7	1.09	0.638	8.77	2.6E-2

Maximum likelihood solutions for various samples, modifications, flow models and values of the Hubble constant. In each case, L_* and C are quoted in terms of $h = H_0/100$ km s^{-1} Mpc^{-1}. A figure in brackets has been fixed to this value while the other parameters are allowed to vary.
Unless otherwise specified, flow model V3 has been used and a Hubble constant of 66 km s^{-1} Mpc^{-1} used in matching directly measured and redshift-derived distances. All normalizations (except solution 21) include an evolutionary correction assuming $\varphi(L, z) = (1+z)^P \varphi(L, z=0)$, $P = 6.7$ (see Section 10). The standard solution is equation (12).

the two power-law forms above. All our resulting sets of maximum likelihood parameters are listed in Table 3.

The parameters quoted here are for the present-epoch 60-μm luminosity function, calculated with flow model V3, $H_0 = 66$ km s^{-1} Mpc^{-1}, $\Omega = 1$, $\Lambda = 0$, using colour-based K-corrections, with density evolution $\varphi(L, z) = (1+z)^{6.7}\varphi(L, 0)$ (see Section 10), and based on the combined samples S1–S7

$$C = (2.6 \pm 0.8) \times 10^{-2}\, h^3\, \mathrm{Mpc}^{-3}$$
$$\alpha = 1.09 \pm 0.120$$
$$\sigma = 0.724 \pm 0.031$$
$$L_* = 10^{(8.47 \pm 0.23)}\, h^{-2}\, L_\odot.$$

The error quoted is the 1σ confidence limit for that parameter when each of the other parameters is varied so as to maximize the likelihood (e.g. Avni 1976). These errors, however, grossly overestimate the total acceptable volume of parameter space. The full 1σ error ellipsoid has principal semi-axes

	$\Delta\alpha$	$\Delta\sigma$	$\Delta \log(L_*/L_\odot)$
Axis 1	0.105	−0.021	0.230
Axis 2	0.057	0.020	−0.020
Axis 3	−0.003	0.010	0.002,

Table 3(b). 1α error ellipses for parametric solutions.

Soln. no.	Sample	$\Delta\alpha$	$\Delta\sigma$	$\Delta\log(L_*/h^{-2}L_\odot)$
1	S1 (Br.Gal.Cat.)	0.65	0.035	1.02
		0.19	0.077	0.12
		0.00	0.030	0.00
2	S2 (Smith et al.)	(0.00)	0.080	(0.00)
3	S3 (NGW)	(0.00)	0.030	(0.00)
4	S4 (Bootes)	(0.00)	0.080	(0.00)
5	S5 (QCD)	0.26	-0.025	0.41
		0.08	0.030	-0.05
		0.00	0.013	0.00
6	S6 (Vader & Simon)	(0.00)	0.080	(0.00)
7	S7 (KKT)	0.10	(0.000)	(0.00)
8	S8 (Large Gal.Cat.)	0.05	(0.000)	(0.00)
9	S9 (PIII)	0.14	(0.000)	0.20
		0.03	(0.000)	0.02
12	S1-S7	0.10	-0.021	0.23
		0.06	0.020	-0.02
		0.00	0.010	0.00
22	S1-S7, Vel > 500kms^{-1}	0.52	-0.004	0.64
		0.07	0.025	-0.05
		0.00	0.009	0.00
24	Cool (<36K),S1-S7	0.09	-0.035	0.18
		0.07	0.019	-0.03
		0.00	0.012	0.00
25	Warm (>36K),S1-S7	0.11	-0.032	0.23
		0.07	0.024	-0.03
		0.00	0.013	0.00
26	L_{fir}, S1-S7	0.13	-0.039	0.29
		-0.08	0.026	0.03
		0.00	0.016	0.00

1σ error ellipsoids for the solutions of Table 3(a), listed as the semi-major axes in parameter space. The errors for solutions 10–21 and 23 are all virtually as for solution 12.

so there is strong correlation between α and L_*, and anti-correlation between them and σ. These correlations are inevitable given the breadth of the luminosity function and the parametric form chosen: a 1σ change along axis 1 leaves the shape of the luminosity function almost unaltered except at very high and low luminosities. The effects of these uncertainties on the luminosity function are shown in Fig. 3.

As explained in Section 5.5, these errors are relative only; that is, they show only which values of the parameters can be ruled out through having a significantly worse likelihood than the best solution. The 'absolute' acceptability of this solution is shown in Fig. 2, where we give the χ^2's between the non-parametric solution for each sample and the overall solution given above; these show that our parametric solution is a reasonable description of the luminosity function for each of the flux-limited surveys.

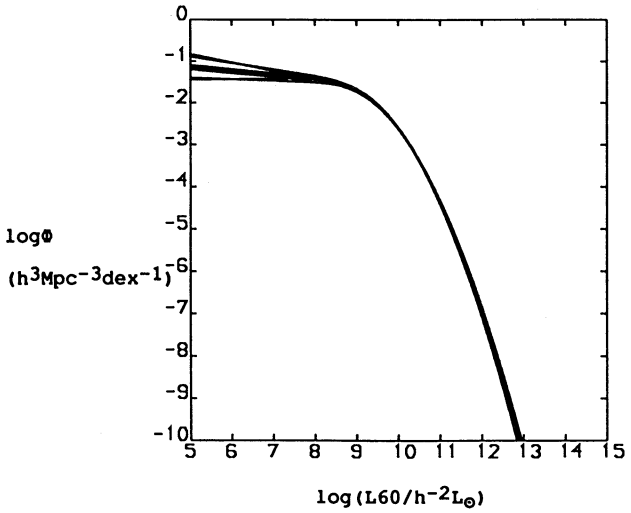

Figure 3. The effect of a 1σ error in the final parametric solution ($H_0 = 66$ km s^{-1} Mpc^{-1}, flow model V3): plotted here is the actual solution together with that obtained by varying the parameters by 1σ in each direction along each of the three principal axes of the error ellipsoid.

The maximum-likelihood parameters can be found for separate samples as long as they have sufficient numbers of sources both above and below L_*; otherwise we can fix one or more parameters to some value and find the maximum-likelihood solution given this constraint. We can then find, for each sample, the acceptability of the final combined solution; we find the final solution to be within the 1σ error ellipsoid for all the flux-limited samples.

6.2 Robustness of the parametric solution

In general, we find our results very insensitive to the flow model used, to the assumed value of the Hubble constant, and to the exclusion of subsets of the data. The various flow models give rise to differences in the detailed behaviour around the knee of the non-parametric luminosity function, but the derived parametric luminosity functions vary negligibly between different flow models, as shown in Fig. 4.

In Fig. 5 we show the effect of using a different Hubble constant. This plot overstates the possible variation; the direct distances are left unaltered, and thus inconsistent with either of the extreme values for the Hubble constant.

Our use of nearby, and especially Local Group, galaxies is perhaps open to question; both the distances and fluxes for some of these are uncertain. In addition, the very lowest luminosity objects are poorly coupled to the rest of the data (although this will always be reflected in the calculated errors). We have therefore calculated a parametric solution excluding the Local Group (Solution 21), and another excluding all galaxies with velocities < 500 km s^{-1} (Solution 22), but the results are not greatly altered. There is also a possible systematic bias due to our use of PSC fluxes for some sources quoted in the PSC as being extended. We have found a solution with the luminosities of such galaxies doubled (Solution 20), which is a very extreme correction, but this has a negligible effect on the derived parameters.

The errors quoted for our luminosity function parameters are statistical only and may still be subject to systematic

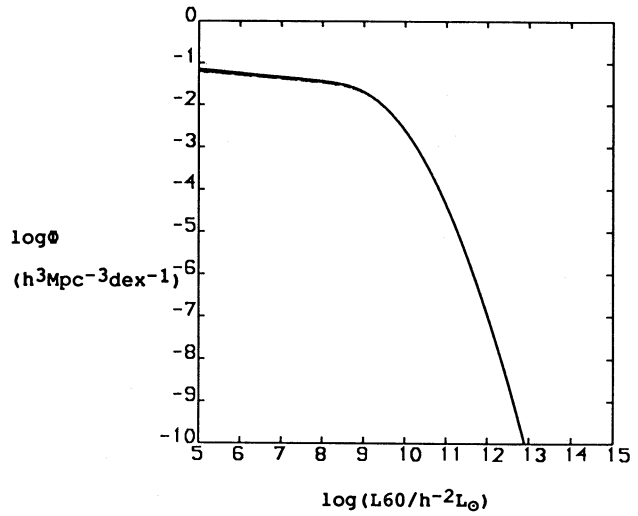

Figure 4. Comparison of the final luminosity function for different flow models; plotted here are the parametric luminosity functions for V2–V7, all calculated with $H_0 = 66$ km s^{-1} Mpc^{-1}.

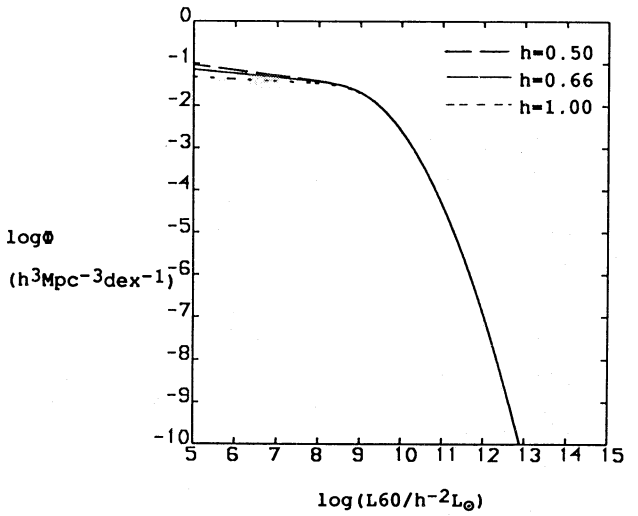

Figure 5. The effect of changing the value of the Hubble constant used in the calculations; plotted here are the parametric solutions calculated with $H_0 = 50, 66, 100$ km s^{-1} Mpc^{-1}.

errors, especially at the faint end. Our results seem robust, and in Section 7 we will provide supporting evidence for a flat faint-end slope. Nevertheless, our quoted errors, and especially that for α, should be treated with caution.

6.3 Comparison with previous results and other parametric forms

A comparison with the two power-law luminosity functions of Paper II and Yahil (1987) is shown in Fig. 6. There is good agreement at luminosities above $10^9\ h^{-2}\ L_\odot$, but the extremely flat form of our function at low luminosities is in strong contrast with previous results.

There are two reasons for this discrepancy. First, in the result of Paper II (where Schmidt's estimator has been used), there is a bias due to very large local density excesses; this is

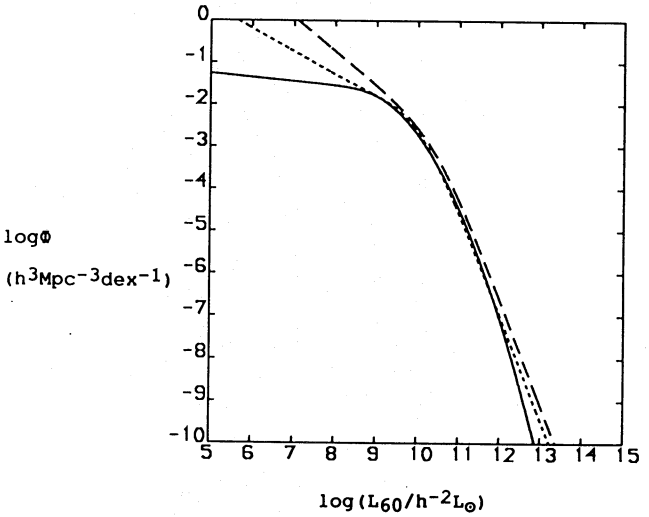

Figure 6. Comparison of our preferred solution ($H_0 = 66$ km s^{-1} Mpc^{-1}, flow model V3, solid line) with that of Paper II (dashed line) and Yahil (1987) (dotted line). All solutions are renormalized to $H_0 = 100\ h$ km s^{-1} Mpc^{-1}. Note that the region of sky used in Paper II has a higher than average surface density of galaxies.

quantified in Section 8. Secondly, we find that the curvature in the luminosity function is spread over a much larger range in luminosity than is the case in a two power-law representation: when combined with a paucity of galaxies of luminosity much below $10^8\ h^{-1}\ L_\odot$ in previous surveys, this forces up the faint-end slope of the luminosity function in order that the knee is well fitted. This effect can be seen clearly in Appendix D, where we give maximum-likelihood solutions to our data set for various other parametric forms. The likelihoods quoted there allow us to formalize our rejection of the alternative parametric forms listed above; the maximum-likelihood solution for each is ruled out at a high significance level as a suitable description of the luminosity function of our data set.

6.4 The 60-μm luminosity functions of populations selected by far-infrared temperature

Given that we have assigned a far-infrared temperature to each source, it is straightforward to find the luminosity function of temperature-selected subsamples. According to the models of Rowan-Robinson & Crawford (1989), sources are starburst/Seyfert or disc-dominated for temperatures above and below 36 K. We have then split the sources into cool ($T_{\rm em} < 36$ K) and warm ($T_{\rm em} \geqslant 36$ K) populations, and calculated their luminosity functions separately. The analytic form above provides a good description for both. The results are shown in Fig. 7 and Table 3.

The overall 60-μm luminosity function is seen to be dominated by normal, cool, galaxies for luminosities below $\sim 5 \times 10^{10}\ h^{-2}\ L_\odot$, and by warm sources above this. There appear to be no cool high-luminosity galaxies, while there are warm galaxies down to very low luminosities. The luminosity function for cool sources is more like an optical luminosity function (i.e. narrower) than that for all sources, but is still very poorly described by a Schechter function.

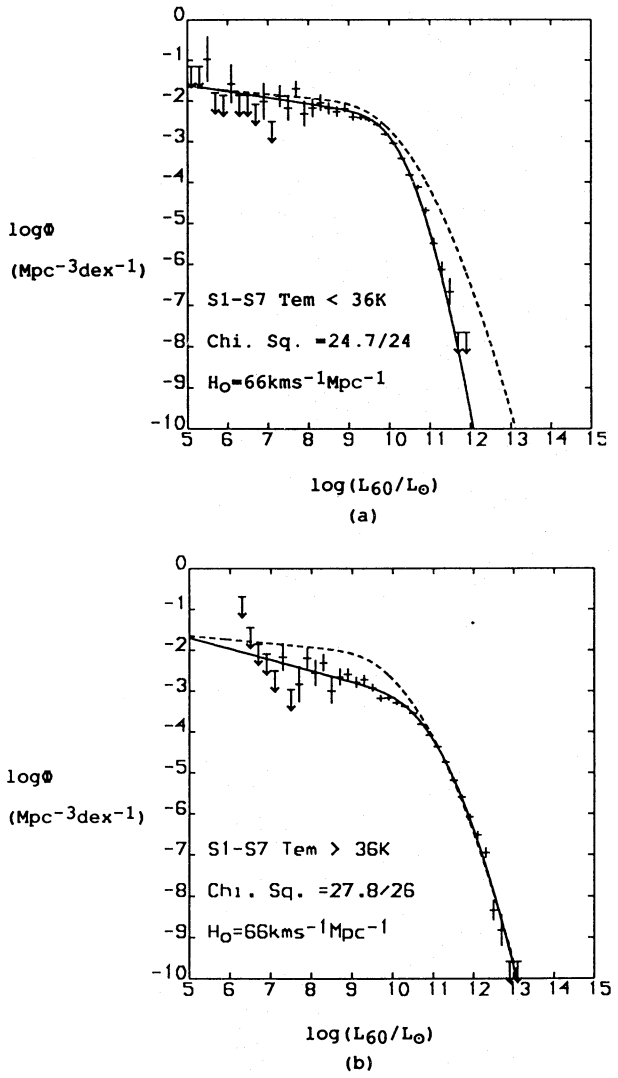

Figure 7. Comparison of non-parametric and parametric luminosity functions for (a) cool ($T_{em} < 36$ K) and (b) warm ($T_{em} \geqslant 36$ K) subsections of the data set, together with the final parametric solution (dashed line). Normalization is from the fraction of our data set in each category. All points and curves are for $H_0 = 66$ km s^{-1} Mpc^{-1}, and flow model V3.

6.5 The far-infrared luminosity function

It is possible to find the integrated far-infrared luminosity function by simply substituting L_{fir} for L_{60} for each galaxy. This does, however, lead to a bias against cold galaxies, as we are still working with 60-μm-selected samples. We have therefore constructed a F_{fir} limited subset of the data as follows.

All of our galaxies have far-infrared temperature greater than 23 K, corresponding to $F_{fir} \leqslant 2.5\, S_{60}\, \nu_{60}$. If we then keep only those sources in each sample with $F_{fir} \geqslant 2.5\, S_{60\,min}\, \nu_{60}$, where $S_{60\,min}$ is the lower 60-μm flux limit for each sample, we can be confident of not losing significant numbers of cold galaxies. This process leaves us with only 1004 sources, but this is enough to find the general shape of the luminosity function. The parametric form used above is an adequate description, and as expected the high-luminosity cut-off is steeper than at 60 μm. We normalize by demanding that the

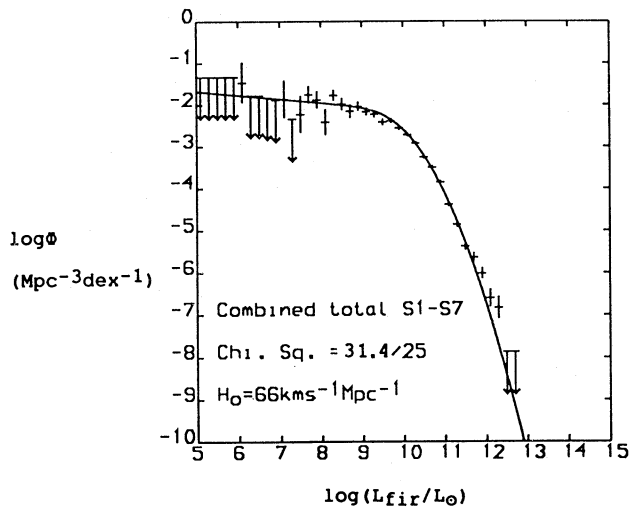

Figure 8. Non-parametric and parametric solutions for the 40–120 μm far-infrared luminosity function, calculated with $H_0 = 66$ km s^{-1} Mpc^{-1} and flow model V3.

number of sources with $F_{fir} \geqslant 1.5$ Jy ν_{60} be 448 sr^{-1}, corresponding to the source counts in the whole *IRAS* galaxy catalog. The non-parametric and parametric solutions are shown in Fig. 8.

6.6 Luminosity densities of *IRAS* galaxies

Our parametric solutions translate to the following local luminosity densities

$$\begin{aligned}
\langle L_{60} \rangle &= (4.2 \pm 0.4) \times 10^7\, h\, L_\odot\ \mathrm{Mpc}^{-3} \\
\langle L_{60}, \mathrm{cool} \rangle &= (2.6 \pm 0.3) \times 10^7\, h\, L_\odot\ \mathrm{Mpc}^{-3} \\
\langle L_{60}, \mathrm{warm} \rangle &= (1.7 \pm 0.2) \times 10^7\, h\, L_\odot\ \mathrm{Mpc}^{-3} \\
\langle L_{fir} \rangle &= (5.6 \pm 0.6) \times 10^7\, h\, L_\odot\ \mathrm{Mpc}^{-3}.
\end{aligned}$$

The uncertainty comes from the source-count normalization, since the variation between different solutions is negligible. These luminosity densities may be compared with that in the blue band

$$\langle L_B \rangle = (1.9 \pm {}^{0.8}_{0.6}) \times 10^8\, h\, L_\odot\ \mathrm{Mpc}^{-3} \quad \text{(Efstathiou } et\ al. \text{ 1988)}.$$

From the above quantities we can find a characteristic optical depth τ for the stars in galaxies: the bulk of the far-infrared luminosity density is due to the absorption and re-emission of starlight, and so we have $\langle L_B \rangle = (\langle L_B \rangle + \langle L_{fir} \rangle) e^{-\tau}$, whence $\tau = 0.26 \pm 0.10$. De Vaucouleurs *et al.* (1976) quote $\tau \sim 0.39$ for spirals; the discrepancy is well explained by the inclusion of ellipticals and lenticulars in the quoted value for $\langle L_B \rangle$.

We also quote the mass-to-infrared luminosity ratio in terms of the density parameter Ω;

$$(M/L_{fir}) = (5000 \pm 500)\, \Omega\, h\, M_\odot/L_\odot$$

although this can, of course, only be true in a statistical sense when averaged over a sufficiently large volume.

7 JOINTLY LIMITED SAMPLES

Samples S8 and S9 have additional optical selection criteria, and neither of the methods of Section 6 can be used directly.

However, they contain relatively large numbers of galaxies at the faint end and knee of the luminosity function respectively, and we have gone to some effort to extract their 60-μm luminosity function reliably.

We have generalized the stepwise maximum-likelihood method to find the non-parametric joint luminosity function $\varphi_2(L_1, L_2)$ of jointly limited samples. We assume φ_2 to be a two-dimensional 'brick-function' in L_1 and L_2, with $\varphi_2 = \varphi_{2j,k}$ in the jth L_1 bin and kth L_2 bin. Equations (5.1) to (5.7) generalize in the obvious way and, as before, 20–30 iterations give good convergence. We collapse the resultant joint luminosity function to find the luminosity functions for L_1 and L_2

$$\varphi(L_1) = \int_{-\infty}^{+\infty} \varphi_2(L_1, L_2)\, d\log L_2,$$
$$\varphi(L_2) = \int_{-\infty}^{+\infty} \varphi_2(L_1, L_2)\, d\log L_1, \qquad (7.1)$$

For these summed functions, there are no meaningful upper limits for empty bins as in Section 5.3.

For S8 (the LGC sample), our optical selection quantity is D_{25}, the blue isophotal angular major diameter. For each galaxy we find D_0, the angular diameter corrected for inclination and internal and galactic extinction as in RC2. This gives us d_i, the linear diameter in parsec, and $d_{\min,i}$, the minimum diameter corresponding to $D_{25} = 8$ arcmin. We then use $L_d = d^2$ as an optical 'luminosity'.

For S9 (the Paper III sample), our optical selection quantity is m_B, the Zwicky magnitude corrected for systematic error as in Kirshner, Oemler & Schechter (1978). For each galaxy we then have the blue luminosity given by $\log(L_B) = 1.97 - 0.4\ M_{B_0}$, where M_{B_0} is the absolute magnitude with inclination, internal extinction and K-correction as in Paper III.

The bivariate luminosity functions are listed in Table 4. Although the statistics are poor, it is clear that both L_d and L_B are well correlated with L_{60}, with $\log L_d$ and $\log L_B$ increasing less fast than $\log L_{60}$. The resultant non-parametric 60-μm luminosity functions are plotted in Fig. 2. We

Table 4. Bivariate optical/60 μm luminosity functions.

$\log(L_d/pc^2)$

$\log(L_{60}/L_\odot)$	6.4	6.8	7.0	7.4	7.8	8.2	8.8	9.2	9.6
5.2		1/1.8							
5.6		1/2.1	1/2.1						
6.0		1/2.1							
6.4									
6.8									
7.2	1/1.9		1/2.3	1/2.8	1/3.1				
7.6			1/2.3	1/2.8	2/2.8				
8.0				1/2.8	1/3.1	2/3.1			
8.4					3/2.6		3/3.4	2/4.2	
8.8					1/3.1	2/3.1	5/3.2	1/4.5	
9.2					2/2.8		2/3.5	4/3.9	1/4.8
9.6						2/3.1	7/3.0	7/3.7	3/4.3
10.0					1/3.1	1/3.4	6/3.1	2/4.2	1/4.8
10.4					1/3.1	1/3.4	1/3.9	2/4.2	
10.8									1/4.8

$\log(L_B/L_\odot)$

$\log(L_{60}/L_\odot)$	8.0	8.4	8.8	9.2	9.6	10.0	10.4	10.8	11.2
7									
7.2	1/1.5								
7.6			1/2.0						
8.0			4/2.2	1/2.8					
8.4			1/3.1	9/2.4	1/3.3	1/3.3			
8.8			3/2.8	26/2.5	23/2.6	7/3.1	1/4.0		
9.2				13/2.8	28/2.7	22/2.8	8/3.3		
9.6					19/2.9	55/2.7	20/3.2	2/4.2	
10.0					4/3.6	26/3.1	42/3.3	7/4.2	
10.4					1/4.2	5/3.8	27/3.6	21/4.2	
10.8						2/4.2	13/3.9	13/4.5	
11.2					1/4.2		1/5.1	4/5.0	1/5.7
11.6									

Bivariate luminosity functions for L_{60} and (a) L_d = (face-on diameter)^2 and (b) L_B = blue luminosity. The number before the slash is $n_{j,k}$, the number of sources in that bin, and the second number is $-\log(\varphi_{j,k})$. The errors in $\log(\varphi_{j,k})$ are always close to $1/\sqrt{n_{j,k}}$. Both sets of numbers are calculated with $H_0 = 66$ km s^{-1} Mpc^{-1} and flow model V3.

find the best fits for our analytic form from these by least-χ^2 fitting; these are listed in Table 3. Although this procedure is inelegant, the results do satisfactorily confirm the flatness of the low end of the luminosity function. Also shown in Fig. 2 are the χ^2 differences between these solutions and our overall best-fitting parametric form; they are rather high but there is no evidence for any systematic deviation.

To parameterize the marginal luminosity functions $\psi(L_1|L_2)$ in the simplest way consistent with the joint luminosity functions, we assume that ψ is Gaussian (in log L_1) with mean linearly dependent on log L_2, $\mu_1 = A_1 + B_1(\log L_2)$, and constant dispersion σ_1. We then find, given $L_{1,i} \geqslant L_{1\,min,i}$ for each source, the values of A_1, B_1 and σ_1 giving the maximum-likelihood solution for the sample. We test the adequacy of these solutions by the Kolmogorov and W^2 tests (Kendall & Stuart 1979) on the probabilities $p(L_1 \geqslant L_{1,i}|L_1 \geqslant L_{1\,\min,i})$, both for the whole data set and for each quartile in L_2. We find adequate fits for $\psi(L_{60}|L_B)$, $\psi(L_{60}|L_d)$, $\psi(L_d|L_{60})$, but not for $\psi(L_B|L_{60})$; here we must introduce a cut-off for L_{60} at $10^{10}\ h^{-2}\ L_\odot$, or use a parabolic dependence for the mean on log L_{60}. The derived parameters vary slightly for different flow models and Hubble constants; the parameters listed in Table 5 are all for $H_0 = 66$ km s^{-1} Mpc^{-1} and flow model V3.

Table 5. Parameters for marginal luminosity functions.

	A	B	σ	$\log L_*$	Kolm/W^2
1. $\psi(L_{60}\|L_d)$	-1.3	1.2	0.75		marginal
2. $\psi(L_d\|L_{60})$	4.9	0.44	0.42		good
3. $\psi(L_{60}\|L_B)$	-2.1	1.15	0.45		good
4. $\psi(L_B\|L_{60})$ ($L_{60}<10^{10}h^{-2}L_\odot$)	3.7	0.65	0.31		fair
5. $\psi(L_B\|L_{60})$ (Parabolic fit)	10.3	0.12	0.29	11.6	fair

Best-fit parameters for the marginal luminosity functions based on samples S8 and S9. In each case we assume $\psi(L_1|L_2)$ to be Gaussian in log L_1 with constant dispersion σ; for 1–4 we assume $\mu = A + B \log L_2$, for 5 we assume $\mu = A + B(\log L_2 - \log L_*)^2$.

In principle we can convolve our marginal luminosity functions with a suitable optical luminosity function to find a parametric 60-μm luminosity function,

$$\varphi_{60}(L_{60}) = \int_{-\infty}^{+\infty} \varphi_{opt}(L_{opt})\,\psi(L_{60}|L_{opt})\,d\log L_{opt}. \qquad (7.2)$$

In general this integral can only be done numerically. Although φ_{60} will keep an approximately power-law/Gaussian form at the high and low ends for either a Schechter or power-law/Gaussian φ_{opt}, this is not true around the knee, and there are no simple relationships between the parameters of ψ and φ_{opt} and those of the best-fitting power-law/Gaussian φ_{60}, except for the faint-end slope. This means that we cannot invert the convolution; there is then no obvious way of assigning a likelihood to a given parameter set for φ_{60}, and we cannot include jointly limited samples in our combined STY solution.

We can, however, employ this procedure to determine the faint-end slope of the 60-μm luminosity function. Use of our $\psi(L_{60}|L_d)$ and the 'diameter function' of Lahav, Rowan-Robinson & Lynden-Bell (1988) leads to a value for α in the range 0.96–1.17; $\psi(L_{60}|L_B)$ and the blue luminosity function of Efstathiou *et al.* (1988) give a value for α of 1.07 ± 0.11; these are in excellent agreement with our minimum-χ^2 derived values.

It is believed that the distribution of $\log(L_{60}/L_B)$ is not Gaussian in general (Paper II; Soifer *et al.* 1984), and we find some evidence for non-linearity in the inverse relationship between L_B and L_{60}. However, we find a linear, Gaussian fit to be an adequate representation of this particular data set. A similar relationship has been obtained for normal galaxies by Feigelson, Isobe & Weedman (1987).

We can use these relationships to investigate whether sample S7 is likely to be incomplete due to galaxies satisfying the 60-μm flux and redshift criteria not being included in the KKT catalogue. A galaxy at 500 km s^{-1} with $S_{60} = 0.6$ Jy will have $L_{60} = 10^{8.0}\ h^{-2}\ L_\odot$. We then have, from $\psi(L_B|L_{60})$ and $\psi(L_d|L_{60})$, 2σ confidence limits for L_B and L_d; these imply a face-on apparent magnitude $m_{B_0} < 13.8$, and face-on diameter $D_0 > 2.9$ arcmin. Nearer galaxies will be brighter and larger than this. It seems unlikely that many such galaxies have been overlooked at $|b| > 20°$, and so our sample should be at least 95 per cent complete. For 3σ we have $m_{B_0} < 14.6$ and $D_0 > 1.8$ arcmin. There are five galaxies out of 68 with one or both of these quantities between 2σ and 3σ below the mean, and none more than 3σ below the mean, in good accordance with expectation. We can then expect that there are very few (if any) galaxies with $S_{60} \geqslant 0.6$ Jy not included in the KKT catalogue because they are too small or faint.

8 MAXIMUM-LIKELIHOOD RADIAL DENSITY DETERMINATION

Just as it is possible to find the shape of the luminosity function independent of density variations, so it is possible to find the density field without knowledge of the luminosity function.

Maximum-likelihood determinations of the luminosity function maximize

$$\mathscr{L} = \Pi \frac{\rho(\boldsymbol{r}_i)\,\varphi(L_i)}{\int \rho(\boldsymbol{r}_i)\,\varphi(L)\,d\log L} = f(L_1,\ldots,L_n|\boldsymbol{r}_1,\ldots,\boldsymbol{r}_n), \qquad (8.1)$$

with the dependence on density cancelling.

If, instead, we integrate over available (comoving) volume rather than available luminosity, the dependence on luminosity function will drop out. That is, we find

$$\mathscr{L}' = \Pi \frac{\rho(\boldsymbol{r}_i)\,\varphi(L_i)}{\int \rho(\boldsymbol{r}_i)\,\varphi(L)\,dV} = f(\boldsymbol{r}_1,\ldots,\boldsymbol{r}_n|L_1,\ldots,L_n). \qquad (8.2)$$

If we parameterize $\rho(\boldsymbol{r})$ and maximize $\mathscr{L}'$ as a function of the parameters, we are finding the density field that makes the observed distribution of redshifts as likely as possible.

To investigate the effects of clustering on $\Sigma 1/V_{max}$ determinations of the luminosity function, we need to find only the radial density distribution, $\rho(|\boldsymbol{r}|)$. Hence we fit $\rho(\boldsymbol{r})$ as an arbitrary step function in z, and maximize

$$\mathscr{L}' = \Pi \frac{\rho(z_i)}{\int_0^{z_{max,i}} \rho(z_i)(dV/dz)\,dz}, \qquad (8.3)$$

where $z_{\max,i}$ is the largest redshift a source could have and still remain in the sample, and V is the comoving volume out to z. For our samples, this involves finding the redshift at which a source at given L_i and $T_{\mathrm{em},i}$ gives a broadband 60-μm flux limit for the sample, using the relativistic, colour and K-corrections of Section 4.

In practice we iterate ρ_j from

$$\frac{\partial \ln \mathscr{L}'}{\partial \rho_j} = \frac{n_j}{\rho_j} - \Sigma \frac{f_{ij} V_j}{V_{\mathrm{eff},i}},$$

where

$$V_{\mathrm{eff},i} = \int_0^{z_{\max,i}} z^2 \rho(z)\, dz, \tag{8.4}$$

V_j is the volume per steradian in the jth bin, f_{ij} is the fraction of the bin available to the source, and the sum is over all sources. As with the luminosity function, we lose the overall normalization; we have set the fractional-variance weighted average density equal to unity, this being equivalent to the source counts. Note that this procedure does not need any adaptation for jointly limited samples, where we use the lower of the redshifts giving the two flux limits, and indeed can be applied to any sample where there is a well-defined maximum distance for inclusion for each source.

There is a very slight dependence on the specific model used for the K-corrections, as this affects the $z_{\max,i}$ found for each source. However, this effect is negligible for the density distributions considered in this section.

Density plots are drawn for each survey in Fig. 9. Each of the groups listed in Table 1(b) represents a very large overdensity, and Virgo shows up clearly in the relevant surveys. There are also large structures revealed at high redshifts; these will be the subject of a future paper.

This density estimator suggests yet another way of calculating luminosity functions: we can adapt Schmidt's method to include the densities found above. That is, for

$$\phi_j =: \frac{1}{\Delta \log(L)} \Sigma \frac{1}{V_{\max,i}} \tag{8.5}$$

[summed over all sources in each $\Delta \log(L)$ bin], we replace $V_{\max,i}$ with $V_{\mathrm{eff}}(z_{\max,i})$ as above, and renormalize from the source counts. This would allow determination of luminosity function with most of the effects of clustering taken out, and not needing any adaptation for jointly limited samples. Although the results are a great improvement on those from Schmidt's method, we find that the z-binning required to make the density estimates sensible is too coarse to eradicate fully the effects of clustering. The method may nevertheless be useful for large samples with a well-defined optical limit but poorly defined relationship between optical and infrared quantities, for example, where a sample suffers from uncertain or variable extinction.

9 $N(z)$ COMPARISON

We have used maximum-likelihood methods to calculate the luminosity function independent of density variations, and to find the radial density distribution independent of the shape of the luminosity function.

From the luminosity function we can find the predicted number of galaxies as a function of redshift, $N_{\mathrm{pr}}(z)$ for any of our samples (the jointly limited samples also require the D–L_{60} or L_{B}–L_{60} relationship). This will not in general look very much like the observed $N_{\mathrm{obs}}(z)$, due to the effects of clustering. The clustering should, however, be described by the $\rho(z)$ we have derived, and so we can divide out the density variations in $N_{\mathrm{obs}}(z)$ to give an 'underlying' $N_{\mathrm{und}}(z)$, i.e.

$$N_{\mathrm{und}}(z) = N_{\mathrm{obs}}(z)/\rho(z). \tag{9.1}$$

This quantity is then both independent of the luminosity function and derived separately for each sample.

In Fig. 10 we show the comparison between $N_{\mathrm{und}}(z)$ and $N_{\mathrm{pr}}(z)$ for each sample. As can be seen, $N_{\mathrm{und}}(z)$ retains no trace of the effects of clustering, even when this is very strong. The agreement with $N_{\mathrm{pr}}(z)$ shows that a single universal $\varphi(L)$ predicts reasonably well the redshift distribution for each sample, and that our D–L_{60} and L_{B}–L_{60} relationships are plausible. The discrepancies are in line with our quoted uncertainties in $\varphi(L)$.

10 EVOLUTION

So far we have ignored the effects of any evolution that may be present in our samples. However, application of the maximum-likelihood radial density estimator of Section 8 to the deepest samples shows a systematic trend to higher densities with redshift (Fig. 11); we interpret this as indicating the presence of strong evolution. Some evidence for evolution at 60 μm has been found in deeper samples (Hacking, Condon & Houck 1987; Lonsdale & Hacking 1989), and what we see is of similar power. A more detailed investigation of *IRAS* evolution will be the subject of a future paper; hence we simply derive limits on the evolutionary content of our present samples and determine its effect on our luminosity function results. To quantify the evolution, we have assumed that the luminosity function evolves according to

$$\varphi_z(L) = g(z)\, \varphi_0[L/f(z)], \tag{10.1}$$

where the subscript refers to epoch, so that we have a combination of density evolution $g(z)$ and luminosity evolution $f(z)$; this model has been used to interpret the radio source counts (e.g. Condon 1984).

None of our samples is deep enough to detect galaxies from the knee of the luminosity function at cosmologically significant distances, so the evolution seen is in the high-luminosity, starburst population only. In addition, because the curvature of the luminosity function is so small at these high luminosities, there is little observational difference between pure density and pure luminosity evolution. Hence we can assume pure density evolution [$f(z) \equiv 1$] and still reproduce the observed evolution. With this assumption, all the maximum-likelihood parameters given in Section 6 and Table 3 are then still correct (because equation 5.1 is still satisfied), whatever the form of $g(z)$, although the normalization is affected. The conclusions of Section 9 are also unchanged because the ratio $N_{\mathrm{pr}}(z)/N_{\mathrm{und}}(z)$ is unaffected. In addition, the assumption of pure density-evolution allows it to be easily quantified: the non-parametric density estimator of Section 8 can be recast into parametric form, with a smooth parametrically defined function $g(z)$ taking the place

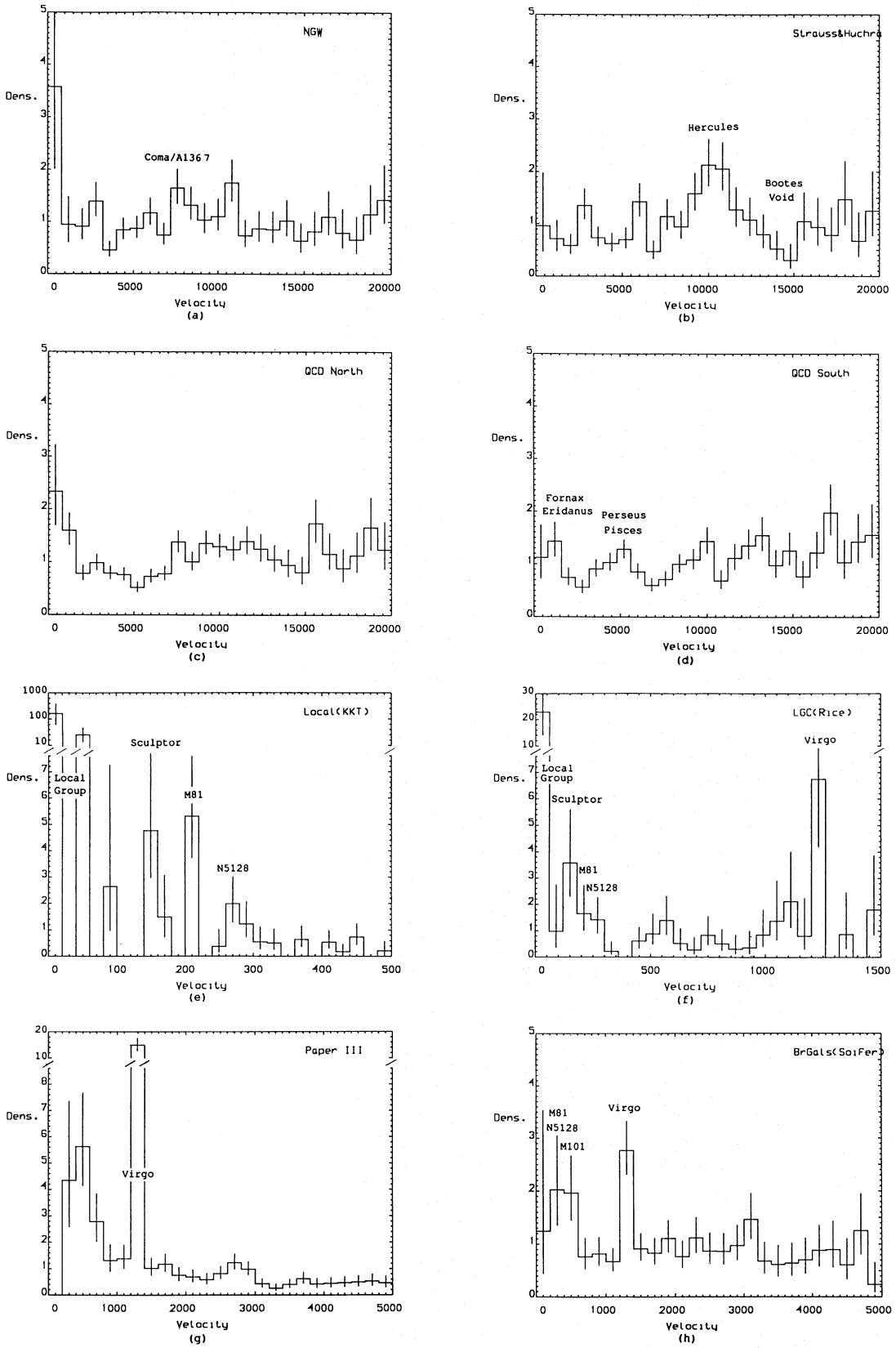

Figure 9. Density against velocity (as corrected using flow model V3) for each sample. Density is from the luminosity-function-independent method. 1 σ errors are shown. Normalization is set by demanding that the fractional-variance-weighted average density be unity, so the units are (density)/(mean density for that sample).

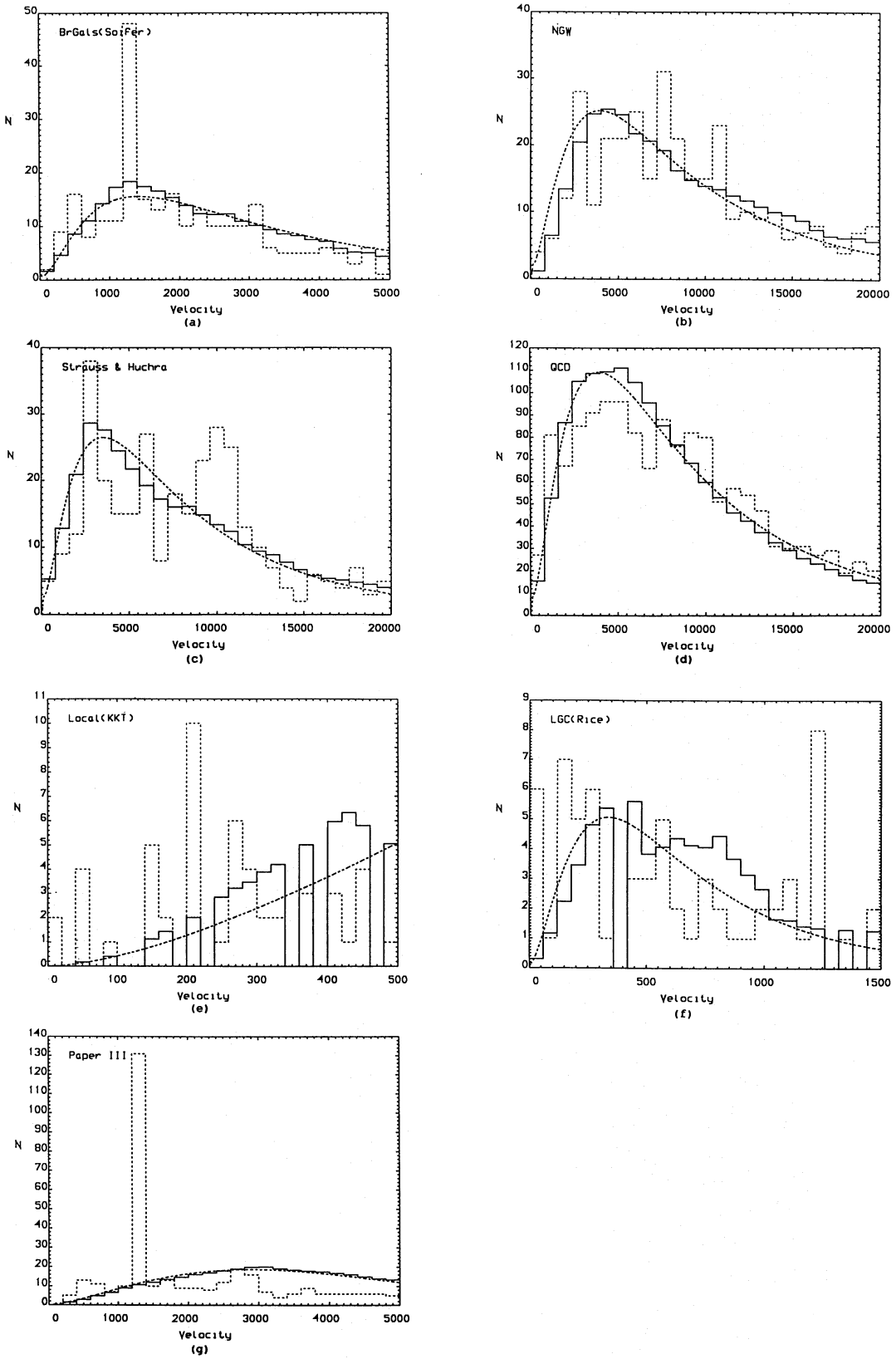

Figure 10. Comparison of observed, underlying and predicted $N(z)$ for each sample. Dotted histogram is observed $N_{\rm obs}(z)$, solid histogram is $N_{\rm und}(z) = N_{\rm obs}(z)/\rho(z)$ as explained in text, curve is $N_{\rm pr}(z)$ from the final luminosity function.

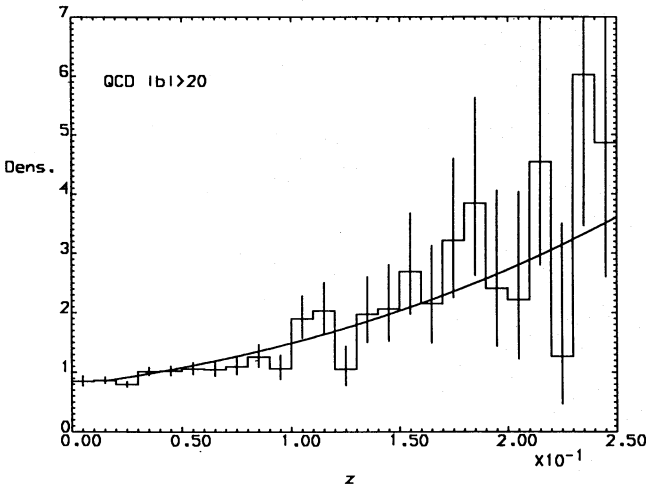

Figure 11. Density distribution against redshift for the QCD survey, on the assumption that the luminosity function does not vary with epoch. The curve shows the predicted behaviour (in an unclustered universe) if in fact $\varphi_z(L)=(1+z)^{6.7}\varphi_0(L)$. Units as Fig. 9.

of the step function $\rho(z)$. We can then find maximum-likelihood solutions for evolution independently of the luminosity function (*cf.* equation 8.2). Local overdensity will mimic (negative) evolution, and hence we introduce a redshift cut-off below $z=0.02$, although this has only a very small effect.

The likelihoods do not depend sufficiently strongly on the parametric form of $g(z)$ to constrain it with any confidence. For the simple form

$$g(z)=(1+z)^P \quad \text{we find} \quad P=6.7\pm2.3 \tag{10.2}$$

and this is the evolutionary correction applied to the normalization throughout the paper unless otherwise stated. The effect of this evolution on $N_{\rm pr}(z)$ for sources with $S_{60}>0.6$ Jy is shown in Fig. 12. Note that the space density of nearby galaxies and the mean and median redshift are all strongly affected.

We can modify this likelihood calculation to include any assumed luminosity evolution; for a given function $f(z)$, we recalculate $z_{\max,i}$ for each source in equation (8.3) to include this luminosity evolution. We can then find, for given $f(z)$, maximum-likelihood solutions for $g(z)$, although we cannot compare likelihoods for different $f(z)$ with this technique. If we assume that luminosities decay exponentially with time (in an $\Omega=1, \Lambda=0$ universe), or

$$L_z=L_0\exp\{\tfrac{2}{3}\,Q[1-(1+z)^{-3/2}]\}, \tag{10.3}$$

then we find P varies with Q such that

$$P+2.1\,Q=6.7\pm2.3, \tag{10.4}$$

so the evolution seen can be explained by invoking pure luminosity evolution of the form above with

$$Q=3.2\pm1.0. \tag{10.5}$$

For such a model we have to recalculate the luminosity function: the best-fitting parameters for the local, present-epoch luminosity function with this value of Q are listed in Table 3, solution (23).

There is also a smaller uncertainty due to the K-corrections; any error in α carries over to an error in Q. However, the results are unaltered if we substitute $\alpha=-2$ for our colour-based model.

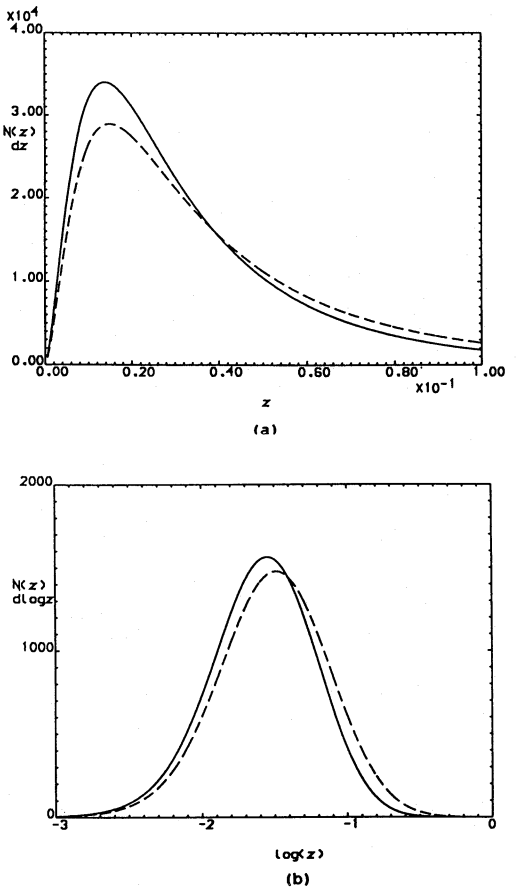

Figure 12. The predicted $N(z)$ distribution per steradian for the whole *IRAS* galaxy catalogue down to 0.6 Jy, without evolution (solid line) and with $g(z)=(1+z)^{6.7}$ as explained in the text (dashed line) for (a) linear and (b) logarithmic redshift increments. Each curve gives a total of 1397 sources per steradian.

The likelihoods for the luminosity function solutions depend very weakly on Q, so there is insufficient evidence to demand any change in the shape of the luminosity function with redshift, and hence we cannot distinguish density from luminosity evolution from this data set.

11 CONCLUSIONS

We have found the 60-μm and far-infrared luminosity functions for *IRAS* galaxies to be well described by an almost constant density per decade in luminosity, for luminosities in the range 10^5–$10^9\ h^{-2}\ L_\odot$, and by a Gaussian dependence on $\log L$ above $10^9\ h^{-2}\ L_\odot$. The shape of the luminosity function is very insensitive to the value of the Hubble constant and to the nature of local bulk flows.

There is no compelling evidence for any variation in luminosity function between the 60-μm surveys published to date. There is strong variation of luminosity function with far-infrared temperature, with the luminosity function of cold sources more nearly resembling an optical luminosity function.

The far-infrared luminosity density of the Universe is about one-third of the blue luminosity density, and is evenly split between cool disc emission and warmer starburst emission.

There is strong evolution present in the *Point Source Catalog,* which must be taken into account both in determining and using the luminosity function.

ACKNOWLEDGMENTS

We are grateful to John Crawford, Ian Parry and especially Xia Xiao Yang for their heroic efforts during the data reduction of the QCD survey. We also thank John Huchra, Marc Davis, Michael Strauss, L. Nicolaci da Costa, Dave Allen and Ray Wolstencroft for provision of pre-publication redshifts. Will Saunders and Andy Lawrence acknowledge the support of an SERC post-graduate studentship and an SERC advanced fellowship, respectively.

REFERENCES

Avni, Y., 1976. *Astrophys. J.,* **210,** 642.
Beichman, C. A., Neugebauer, G., Habing, H. J., Clegg, P. E. & Chester, T. J., 1984. IRAS *Explanatory Supplement* (JPL D-1855).
Condon, J. J., 1984. *Astrophys. J.,* **287,** 461.
Davis, M. & Strauss, M. A., 1988. In: *Comets to Cosmology, Proceedings of the 3rd* IRAS *Conference,* A. Lawrence (Ed.), Springer-Verlag, Berlin.
de Vaucouleurs, G. H., de Vaucouleurs A. & Corwin, H. G., 1976. *Second Reference Catalogue of Bright Galaxies,* University of Texas Press, Austin.
Efstathiou, G. P., Ellis, R. S. & Peterson, B. A., 1988. *Mon. Not. R. astr. Soc.,* **232,** 431.
Faber, S. M. & Burstein, D., 1987. In: *Large Scale Motions in the Universe, Proceedings of the Pontifical Academy of Sciences Study Week No. 27,* eds Coyne, G. & Rubin, V. C., Princeton University Press, Princeton.
Feigelson, E. D., Isobe, T. & Weedman, D. W., 1987. *Astrophys. J.,* **319,** L51.
Hacking, P. B., Condon, J. J. & Houck, J. R., 1987. *Astrophys. J.,* **316,** L15.
Harmon, R. T., Lahav, O. & Meurs, E. J. A., 1987. *Mon. Not. R. astr. Soc.,* **228,** 5P.
Huchtmeier, W. K. & Richter, O. G., 1986. *Astr. Astrophys. Suppl.,* **63,** 323.
IRAS *Point Source Catalog,* Version 2, 1988. Joint *IRAS* Working Group, GPO, Washington, DC.
IRAS *Small Scale Structure Catalog,* 1988. Prepared by Helou, G. & Walker, D., GPO, Washington, DC.
Kendall, M. G. & Stuart, A., 1979. *The Advanced Theory of Statistics, Vol. 2,* 4th edn, Charles Griffin, London
Kirschner, R. P., Oemler, A. & Schechter, P. L., 1978. *Astr. J.,* **83,** 1549.
Kraan-Kortweg, R. C. & Tammann, G. A., 1980. *Astr. Nachr.,* **300,** 181.
Lahav, O., Rowan-Robinson, M. & Lynden-Bell, D., 1988. *Mon. Not. R. astr. Soc.,* **234,** 677.
Lawrence, A., Rowan-Robinson, M., Leech, K., Jones, D. H. P. & Wall, J. V., 1989. *Mon. Not. R. astr. Soc.,* **240,** 329.
Lawrence, A., Walker, D., Rowan-Robinson, M., Leech, K. J. & Penston, M. V., 1986. *Mon. Not. R. astr. Soc.,* **219,** 687 (Paper II).
Leech, K. J., Lawrence, A., Rowan-Robinson, M., Walker, D. & Penston, M. V., 1988. *Mon. Not. R. astr. Soc.,* **231,** 977 (Paper IV).
Lonsdale, C. J. & Hacking, P. B., 1989. *Astrophys. J.,* **339,** 712.
Lubin, P. & Villela, T., 1986. In: *Galaxy Distances and Deviations from Universal Expansion,* eds Madore, B. F. & Tully, R. B., Reidel, Dordrecht.
Nicoll, J. F. & Segal, I. E., 1983. *Astr. Astrophys.,* **118,** 180.
Rice, W., Lonsdale, C. J., Soifer, B. T., Neugebauer, G., Koplan, E. L., Lloyd, L. A., de Jong, T. & Habing, H. J., 1988. *Astrophys. J. Suppl.,* **68,** 91 (*The Large Galaxy Catalog*).
Richter, O. G., Tammann, G. A. & Huchtmeier, W. K., 1987. *Astr. Astrophys.,* **171,** 33.
Rowan-Robinson, M., 1988. In: *Comets to Cosmology, Proceedings of the 3rd* IRAS *Conference,* ed. Lawrence, A., Springer-Verlag, Berlin.
Rowan-Robinson, M., 1989. *Space Sci. Rev.,* **48,** 1.
Rowan-Robinson, M. & Crawford, J., 1989. *Mon. Not. R. astr. Soc.,* **238,** 523.
Rowan-Robinson, M., Helou, G. & Walker, D., 1987. *Mon. Not. R. astr. Soc.,* **227,** 589 (Paper III).
Rowan-Robinson, M., Walker, D., Chester, T., Soifer, T. & Fairclough, J., 1986. *Mon. Not. R. astr. Soc.,* **219,** 273 (Paper I).
Sandage, A., Binggeli, B. & Tammann, G. A., 1985. *Astr. J.,* **90,** 1759.
Sandage, A., Tammann, G. A. & Yahil, A., 1979. *Astrophys. J.,* **232,** 352.
Sanders, D. B., Soifer, B. T., Elias, J. H., Madore, B. F., Matthews, K., Neugebauer, G. & Scoville, N. Z., 1988. *Astrophys. J.,* **325,** 74.
Schmidt, M., 1968. *Astrophys. J.,* **151,** 393.
Smith, B. J., Kleinmann, S. G., Huchra, J. P. & Low, F. J., 1987. *Astrophys. J.,* **318,** 161.
Soifer, B. T. *et al.* 1984, *Astrophys. J.,* **278,** L71.
Soifer, B. T., Sanders, D. B., Neugebauer, G., Danielson, G. E., Lonsdale, C. J., Madore, B. F. & Persson, S. E., 1986. *Astrophys. J.,* **303,** L41.
Soifer, B. T., Sanders, D. B., Madore, B. F., Neugebauer, G., Danielson, G. E., Elias, J. H., Persson, C. F. & Rice, W. L., 1987. *Astrophys. J.,* **320,** 238.
Strauss, M. A. & Huchra, J., 1988. *Astr. J.,* **95,** 1602.
Tammann, G. A. & Sandage, A., 1985. *Astrophys. J.,* **294,** 81.
Vader, J. P. & Simon, M., 1987. *Astr. J.,* **94,** 854.
Yahil, A., 1987. In: *Large Scale Motions in the Universe, Proceedings of the Pontifical Academy of Sciences Study Week No. 27,* eds Coyne, G. & Rubin, V. C., Princeton University Press, Princeton.

APPENDIX A: COLOUR AND IDENTIFICATION CONSTRAINTS USED IN SELECTING SAMPLES

(1) Sources in the PSC version 2, with a detection at 60 μm and without counterparts in the SSSC, are included provided that they satisfy the following criteria:

(a) $\mathrm{Log}(S_{60}/S_{25}) > -0.5$: this excludes most stars, but no catalogued galaxies.

(b) For sources detected at 25 μm, $\log(S_{25}/S_{12}) < 1.0$, or source is identified with a known galaxy. This condition excludes planetary nebulae but only two known galaxies have to be re-instated (Arp 220 and NGC 4418); no other objects above $|b| > 10°$ are excluded.

(c) For sources detected at 25 and 100 μm, then $\log(S_{100}/S_{25}) > -0.3$. This excludes 12 stars and planetary nebulae, but no catalogued galaxies.

(d) $\mathrm{Log}(S_{100}/S_{60}) < 0.6$, or source is identified with a catalogued galaxy. This condition excludes cirrus, while experience at high latitude has shown that there can be very few uncatalogued galaxies with $S_{60} \geqslant 0.6$ Jy cool enough to violate this condition.

(e) There is not a sole identification with a star, planetary nebula or star cluster.

(f) They are not associated with Local Group galaxies or other nearby galaxies included in the catalogue of Rice *et al.* (1988).

Where only an upper limit is known for a flux in any band, this is used above except where otherwise specified.

(2) Where a PSC source has an identification with a

catalogued galaxy and a corresponding entry in the SSC, the latter flux is used if it is larger. Sources in the SSC without PSC counterparts are also included if there is a galaxy identification.

(3) Galaxies in the *Large Galaxy Catalog* (Rice *et al.* 1988) have been included (and the associated point sources deleted).

These conditions and the reliability of the resulting catalogue are discussed further in Rowan-Robinson (1988) and Rowan-Robinson & Saunders, in preparation.

APPENDIX B: FLOW MODELS USED

V1: No infall corrections. Galaxies without directly measured distances are taken to have distance V/H_0, where V is the velocity with respect to the centroid of the Local Group.

V2: Linear Virgo infall only. $V_V \propto d_V^{-1}$, where V_V is the infall towards Virgo for a galaxy at distance d_V from Virgo. $V_V = V_{V,LG} = 220$ km s^{-1} at the Local Group (Tammann & Sandage 1985), where $d_V = d_{V,LG} = 19.0$ Mpc (Rowan-Robinson 1989). Galaxies in the triple-valued zone are put at the Virgo distance.

V3: As V2, but with a Microwave Background contribution of 600 km s^{-1} towards $(l, b) = (268, 27)$ (Lubin & Villela 1986). This is blended in smoothly between $d_{V,LG}$ and $3d_{V,LG}$ from the Local Group, such that galaxies at large distances are at rest with respect to the MWB.

V4: As V2, but with $V_{V,LG} = 100$ km s^{-1}, and an additional 'Great Attractor' infall V_{GA} towards $(l_{GA}, b_{GA}) = (308, 18)$, $d_{GA,LG} = 3d_{V,LG}$. The infall at the Local Group is taken to be 500 km s^{-1}, and $V_{GA} \propto d_{GA}^{-1}$. The coordinates are from Faber & Burstein (1987), while the distance is in line with that found by Davis & Strauss (1988).

V5: Faber & Burstein's Model 3 (1987) based on elliptical galaxies. Their 'local anomaly' has not been modelled, but most of our distances in this region are from direct indicators in any case.

V6: As V4 but with a Great Attractor infall of 250 km s^{-1} only, more in line with the analysis of the *IRAS* dipole by Lahav *et al.* (1988) and Harmon, Lahav & Meurs (1987).

V7: As V6 but with a residual MWB contribution as in V3.

APPENDIX C: ESTIMATION OF 100-μm FLUX FOR SOURCES WITH ONLY UPPER LIMITS

We assume that $R_{34} = \log(S_{60}/S_{100})$ is adequately described as a normal distribution with mean $A + B(\log L_{60}/L_\odot)$ and constant standard deviation, where L_{60} is for the moment calculated from S_{60} with a K-correction of $\alpha = -2$. We use all sources with 60-μm fluxes greater than 1 Jy (of which all but 37 out of 1891 have good- or moderate-quality fluxes at 100 μm) to make this fit. Sources with an upper limit at 100 μm have a lower limit to R_{34}, and we put R_{34} equal to the expected value for the distribution given this lower limit. We then have an estimate for S_{100}. The derived parameters for the distribution of R_{34} depend very slightly on flow model; for model V3 they are

$A = -1.17$, $B = 0.082$ with dispersion in R_{34} of $\sigma = 0.13$.

APPENDIX D: MAXIMUM LIKELIHOOD SOLUTIONS FOR OTHER PARAMETRIC FORMS

We have found best-fitting parameters and likelihood ratios (in terms of the likelihood for the power law/Gaussian solution, $\mathscr{L}_{pg}$) for various parametric forms. All solutions are for samples S1–S7, flow model V3 and $H_0 = 66$ km s^{-1} Mpc^{-1}. The second line in each case is the solution when galaxies within 500 km s^{-1} are excluded.

	α	β or σ	$\log(L_*/h^{-2}L_\odot)$	$\ln(\mathscr{L}/\mathscr{L}_{pg})$
Power law/Gaussian	1.09	0.724	8.47	0.00
	0.91	0.726	8.23	0.00
Differential two-power law	1.21	2.18	9.61	−4.16
	1.34	2.11	9.74	−3.92
Cumulative two-power law	0.38	1.88	9.38	−7.75
	0.52	1.83	9.55	−5.63
(log)Gaussian	—	0.800	7.98	−8.22
	—	0.725	8.37	−0.22
Schechter	2.03	—	11.2	−87.0
	2.18	—	11.3	−51.4

The parametric forms are

Differential two-power law (Lawrence *et al.* 1986):

$$\varphi(L) = C\left(\frac{L}{L_*}\right)^{-\alpha}\left(1+\frac{L}{\beta L_*}\right)^{-\beta}$$

Cumulative two-power law (Yahil 1987):

$$\Phi(L) = C\left(\frac{L}{L_*}\right)^{-\alpha}\left(1+\frac{L}{\beta L_*}\right)^{-\beta}$$

Gaussian:

$$\varphi(L) = C\exp-\left(\frac{\log^2(L/L_*)}{2\sigma^2}\right)$$

Schechter:

$$\varphi(L) = C\left(\frac{L}{L_*}\right)^{\alpha}\exp-\left(\frac{L}{L_*}\right).$$

In each case $\varphi(L) = -d\Phi(L)/d\log L$, where $\Phi(L)$ is the number density of galaxies brighter than L.

For two solutions φ and φ' with m and m' parameters and likelihoods $\mathscr{L}$ and $\mathscr{L}'$, the difference in likelihoods is significant at the $\nu\sigma$ level, where

$\nu = 2[(m'-m) - \ln(\mathscr{L}'/\mathscr{L})]$ (e.g. Kendall & Stuart 1979).

Hence the Schechter and both two-power law forms are not acceptable, while a Gaussian is a satisfactory description once the very lowest luminosity galaxies have been excluded.